# Spatial Modulation for Joint Radar-Communications Systems: Design, Analysis, and Hardware Prototype

Dingyou Ma ⓘ, Nir Shlezinger, *Member, IEEE*, Tianyao Huang ⓘ, Yariv Shavit, Moshe Namer, Yimin Liu ⓘ, *Member, IEEE*, and Yonina C. Eldar ⓘ, *Fellow, IEEE*

*Abstract*—**Dual-function radar-communications (DFRC) systems implement radar and communication functionalities on a single platform. Jointly designing these subsystems can lead to substantial gains in performance as well as size, cost, and power consumption. In this paper, we propose a DFRC system, which utilizes generalized spatial modulation (GSM) to realize coexisting radar and communications waveforms. Our proposed GSM-based scheme, referred to as spatial modulation based communication-radar (SpaCoR) system, allocates antenna elements among the subsystems based on the transmitted message, thus achieving increased communication rates by embedding additional data bits in the antenna selection. We formulate the resulting signal models, and present a dedicated radar processing scheme. To evaluate the radar performance, we characterize the statistical properties of the transmit beam pattern. Then, we present a hardware prototype of the proposed DFRC system, demonstrating the feasibility of the scheme. Our results show that the proposed GSM system achieves improved communication performance compared to techniques utilizing fixed allocations operating at the same data rate. For the radar subsystem, our experiments show that the spatial agility induced by the GSM transmission improves the angular resolution and reduces the sidelobe level in the transmit beam pattern compared to using fixed antenna allocations.**

*Index Terms*—**Joint radar-communications system, spatial modulation.**

## I. INTRODUCTION

A WIDE variety of systems, ranging from autonomous vehicles to military applications, implement both radar and communications. Traditionally, these two functionalities are designed independently, using separate subsystems. An alternative strategy, which is the focus of growing research attention, is to *jointly design* them as a dual function radar-communications (DFRC) system [2]–[6]. Such joint designs improve performance by facilitating coexistence [3], as well as contribute to reducing the number of antennas [4], system size, weight, and power consumption [7].

A common approach for realizing DFRC systems utilizes a single dual-function waveform, which is commonly based on traditional communications signaling, or on an optimized joint waveform [8]–[10]. The application of orthogonal frequency division multiplexing (OFDM) communication signaling for probing was studied in [8], while employing spread spectrum waveforms for DFRC systems was considered in [11]. The usage of such signals, which were originally designed for communications, as dual function waveforms, inherently results in some performance degradation [12]. For instance, using OFDM signaling leads to waveforms with high peak-to-average-power ratio, which induces distortion in the presence of practical power amplifiers, and limits the radar detection capability in short ranges [13]. Multiple-input multiple-output (MIMO) radar, which transmits multiple waveforms simultaneously, facilitates designing optimized dual-function waveforms [9], [10]. These optimized waveforms balance the tradeoff between communication and radar performance in light of the constraints imposed by both systems. However, such joint optimizations require prior knowledge of the communication channel and the radar targets, which is likely to be difficult to acquire in dynamic setups, and typically involves solving a computationally complex optimization problem.

When radar is the primary user, a promising DFRC method is to embed the message into the radar waveform via index modulation (IM) [14]. IM is a promising communication technique with high spectral and energy efficiency. In IM, information is embedded into the indices of certain transmission building blocks, including transmit antennas [15], subcarriers [16], and spreading codes [17]. An additional form of IM coveys the communication message via the indices of multiple building blocks, e.g., by jointly embedding information into the indices of the spreading code and the active antennas [18]–[20]. This concept is employed to design the DFRC system. In MIMO radar, IM can be realized by conveying the information in the radar sidelobes [21], using frequency hopping waveforms [22], and in the permutation of orthogonal waveforms among the elements [23]. Recently, the work [24] proposed the IM-based multi-carrier agile joint radar communication (MAJoRCom) system, which embeds the communication message into the transmission parameters of frequency and spatially agile radar waveforms. While these techniques induce minimal effect on

Dingyou Ma, Tianyao Huang, and Yimin Liu are with the EE Department, Tsinghua University, 100084 Beijing, China (e-mail: mdy16@mails.tsinghua.edu.cn; huangtianyao@tsinghua.edu.cn; yiminliu@tsinghua.edu.cn).

Nir Shlezinger is with the School of ECE, Ben-Gurion University of the Negev, 8410501 Be'er-Sheva, Israel (e-mail: nirshl@bgu.ac.il).

Yariv Shavit and Yonina C. Eldar are with the Faculty of Math and CS, Weizmann Institute, 7610001 Rehovot, Israel (e-mail: yariv.shavit@gmail.com; yonina.eldar@weizmann.ac.il).

Moshe Namer is with the EE Department, Technion 3200003 Haifa, Israel (e-mail: namer@ee.technion.ac.il).

Digital Object Identifier 10.1109/TVT.2021.3056408

radar performance, they typically result in low data rates compared to using dedicated communication signals.

DFRC strategies utilizing a single waveform inherently induce performance loss on either its radar functionality, as in OFDM waveform based methods, or lead to a low communication rate, which is the case with the radar waveform based MA-JoRCom. An alternative DFRC strategy is to utilize independent radar and communication waveforms, allowing each functionality to utilize its suitable signaling method. When using individual waveforms, one should facilitate coexistence by controlling their level of mutual interference. This can be achieved by using fixed non-overlapping bands and antennas [4], as well as by efficiently allocating bandwidth resources between the subsystems [25]. In MIMO radar, coexistence can be achieved by beamforming each signal in the proper direction [26], [27] as well as by using spectrally and spatially orthogonal waveforms [10]. The resulting tradeoff between radar and communication of this strategy stems from their mutual interference as well as the resource sharing between the subsystems, in terms of spectrum, power, and antennas.

In this work we propose a spatial modulation based communication-radar (SpaCoR) system, which implements a mixture of individual radar and communications waveforms with IM via generalized spatial modulation (GSM) [15], [28]. GSM combines IM, in which data is conveyed in the transmission parameters, with dedicated communications signaling. As such, the proposed approach exhibits only a minor degradation in radar performance due to the presence of data transmission, as common in IM based DFRC systems [2], while supporting the increased data rates with individual waveforms. We demonstrate the feasibility of SpaCoR by presenting a hardware prototype which implements this scheme.

In particular, we consider a system in which radar and communications use different fixed bands, thus complying with existing standardization. To avoid the hardware complications associated with transmitting multiband signals, we restrict each antenna element to transmit only a single waveform, either radar or communications. To maximize the performance under these restrictions, the proposed method allocates the antenna array elements between the radar and communications subsystems, which operate at different bands thus avoiding mutual interference. The allocation is based on the transmitted message using GSM, thus embedding some of the data bits in the antenna selection, inducing spatial agility [29]. As the communications subsystem is based on conventional GSM, for which the performance was theoretically characterized in [30], we analyze only the radar performance of SpaCoR. In particular, we prove that its agile profile mitigates the degradation in radar beam pattern due to using a subset of the antenna array, which in turn improves its accuracy over approaches with a fixed antenna allocation.

We implement SpaCoR in a specifically designed hardware prototype utilizing a two-dimensional antenna with 16 elements, demonstrating the practical feasibility of the proposed DFRC system. Our prototype allows to evaluate SpaCoR using actual passband waveforms with over-the-air signaling. In our experimental study, we compare SpaCoR to DFRC schemes using individual subsystems with fixed antenna allocation. Our results show that the communications subsystem of SpaCoR achieves improved bit error rate (BER) performance compared to the fixed allocation system when using the same data rate. For the radar subsystem, our experiments show that spatial agility of SpaCoR leads to improved angular resolution.
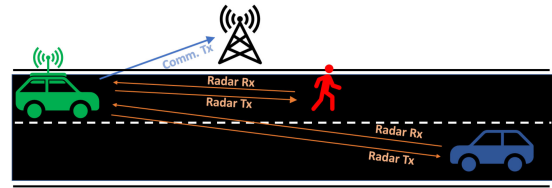


Fig. 1.    An autonomous vehicle with radar and communications functionalities.

The rest of the paper is organized as follows: Section II presents the system model, detailing the communications and radar subsystems. Section III analyzes the radar transmit beam pattern. The high level design of the DFRC system prototype is described in Section IV, and the implementation of each of its components is detailed in Section V. We evaluate the performance of the proposed system in a set of experiments in Section VI. Finally, Section VII provides concluding remarks.

The following notations are used throughout the paper: Boldface lowercase and uppercase letters denote vectors and matrices, respectively. We denote the transpose, complex conjugate, Hermitian transpose and integer floor operation as $(\cdot)^T$, $(\cdot)^*$, $(\cdot)^H$ and $\lfloor \cdot \rfloor$, respectively. The complex normal distribution with mean $\mu$ and variance $\sigma^2$ is expressed as $\mathcal{CN}(\mu, \sigma^2)$, while $\mathcal{E}\{\cdot\}$ and $\mathcal{V}\{\cdot\}$ are the expected value and variance of a random argument, respectively. The sets of complex and natural numbers are $\mathbb{C}$ and $\mathbb{N}$, respectively.

## II. SpaCoR System Model

Here, we detail the proposed SpaCoR system. To that aim, we first discuss the main guidelines and model constraints under which the system is designed in Section II-A. Then, in Section II-B we present the overall DFRC method, and elaborate on the individual communications and radar subsystems in Sections II-C–II-D, respectively.

### A. System Design Guidelines and Constraints

We consider a system equipped with a phased array antenna implementing active radar sensing while communicating with a remote receiver. An illustration of such a system in the context of vehicular applications is given in Fig. 1. In the DFRC system, radar is the primary user and communications is the secondary user. We consider a pulse radar, in which the transmission and reception are carried out in a time-division duplex manner. The communication signal is transmitted during radar transmission. Only the communications receiver is required to have channel state information (CSI), while the DFRC transmitter can be ignorant of the channel realization.

We require the radar and communication functionalities to operate on the same antenna array without mutual interference. An intuitive approach to implement such orthogonality is by time sharing. However, for many applications, radar needs to work continuously in time, rendering time sharing irrelevant. An alternative approach is to boost spatial orthogonality by beamforming, as in, e.g., [26], [27]. However, these approaches typically require fully configurable MIMO arrays as well as knowledge of the communication channel. Consequently, we set the subsystems to use non-overlapping frequency bands, allowing these functionalities to work simultaneously in an
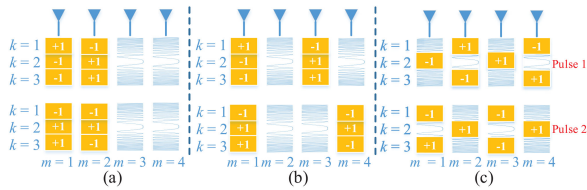
Fig. 2. Illustration of the fixed antenna allocation schemes and SpaCoR. The chirplet waveform represents radar transmission while ±1 denotes a communication symbol. (a) *Fix1*: The antenna array is divided into two sub-ULAs, and the allocation pattern remains static. (b) *Fix2*: The allocation pattern changes randomly between different radar pulses. (c) SpaCoR: Here, the allocation varies between symbol time slots.

orthogonal fashion while complying with conventional communication standards and spectral allocations.

Finally, in order to maintain high power efficiency, we avoid the transmission of multiband signals. Consequently, each antenna element can only be utilized for either radar or communications signalling at a given pulse repetition interval (PRI). By doing so, each element transmits narrowband signals, avoiding the envelop fluctuations and reduction in power efficiency associated with multiband signaling [29].

To summarize, our system is designed to comply with the following guidelines and constraints:

- Radar is based on pulse probing.
- The same array element cannot be simultaneously used for both radar and communications transmission.
- Both functionalities transmit at the same time, and the returning radar echoes are captured in the complete array.
- The waveforms are orthogonal in spectrum.

An intuitive design approach in light of the above constraints is to divide the antenna array into two fixed sub-arrays, each assigned to a different subsystem, resulting in separate systems. Nonetheless, we next show that performance gains in both radar and communications can be achieved using a joint design, which guarantees a low complexity structure, while complying with the aforementioned constraints.

### B. SpaCoR System

To formulate the proposed DFRC method, we first elaborate on the drawbacks of using fixed allocation, after which we discuss how these drawbacks are tackled in our joint design. We focus on systems equipped with a uniform linear array (ULA) consisting of $M$ antenna elements with inter-element spacing $d$. The antenna array is a one-dimensional element-level digital array, where the transmit waveforms are generated digitally for each element, facilitating beamforming in digital baseband. While here we focus on one-dimensional arrays for ease of presentation, our prototype detailed in Section IV uses a two-dimensional antenna surface.

As mentioned in the previous subsection, an intuitive approach is to divide the antenna elements between radar and communications in a fixed manner such that the antenna allocation pattern is static during each radar pulse duration. One simple fixed allocation scheme is obtained by dividing the antenna array into two sub-ULAs, referred to henceforth as *Fix1* and illustrated in Fig. 2(a). Another fixed allocation approach randomly divides the antenna array into two sub-arrays while allowing the allocation pattern to change between different radar pulses. This technique is referred to as *Fix2*, and is illustrated in Fig. 2(b). In these fixed antenna allocation methods, during each

pulse transmission, $K$ symbols are transmitted from the antenna elements assigned to communications. In the example in Fig. 2, two antenna elements are allocated for communication in a static manner during each radar pulse, and each element transmits $K = 3$ symbols during one radar pulse, while the remaining two elements are allocated to radar.

These fixed allocation techniques affect the performance of both radar and communications. Compared with traditional phased array radar utilizing all the elements for radar transmission, using a fixed sub-array yields a wider mainlobe or higher sidelobes in the transmit beam pattern, which are shown in Section III. For the communications subsystem, fixed allocation does not exploit the fact that the system is equipped with a larger number of elements than what is actually utilized, and the data rate can be increased by exploiting the spatial diversity.

To exploit the full antenna array for both radar and communications, we propose a DFRC scheme which randomly allocates the antenna elements between radar and communications. During transmission, the antenna allocation is changed between different symbol slots. Inspired by GSM communications [15], [28], the selection of the specific antennas is determined by some of the bits intended for transmission.

SpaCoR overcomes both the radar and communications drawbacks of using fixed allocation schemes: For the radar subsystem, each element is effectively used for probing with high probability over a large number of time slots, which results in a transmit beam pattern approximating the beam pattern of the full antenna array. In fact, as we show in our analysis in Section III, the resulting expected beam pattern approaches that achieved when using the full array for radar. For the communication functionality, additional bits are conveyed in the selection of the antennas. These additional bits increase the data rate, or alternatively, allow the usage of sparser constellations in the dedicated waveform compared to fixed allocation with the same data rate. An illustration of the resulting waveform is depicted in Fig. 2(c). In this example, two antennas are allocated for communication at every time instance. The information bits are conveyed by the combination of the communications antennas and via the signals transmitted from them, as detailed in the sequel.

### C. Communications Subsystem

The proposed communications subsystem, which utilizes dedicated waveforms while allowing extra information bits to be conveyed in the selection of transmit antennas, implements GSM signaling [15], [28]. Therefore, to formulate the communications subsystem, we start with a brief review of GSM, after which we discuss how the received symbols are decoded.

*1) Generalized Spatial Modulation:* GSM, originally proposed in [28], combines spatial IM with multi-antenna transmission, aiming at increasing the data rate when using a subset of the antenna array elements. As such, GSM refers to a family of IM-based methods. Our proposed DFRC system specifically builds upon the GSM scheme of [15], as detailed next.

The information bits conveyed in each GSM symbol are divided into spatial selection bits and constellation bits. The spatial selection bits determine the indices of the transmit antennas. By letting $M_T^c < M$ be the number of antennas used for communications transmission, it holds that there are $\binom{M}{M_T^c}$ different possible antenna combinations. As a result, $\lfloor \log_2 \binom{M}{M_T^c} \rfloor$ bits can be conveyed through the antenna selection in each GSM
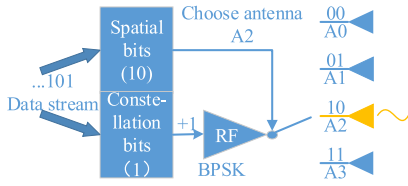
Fig. 3.    GSM transmission illustration.

symbol. The selected antennas are used to transmit the symbols embedding the constellation bits. While, in general, GSM can be combined with any form of signaling [15], we focus on phase shift keying to maintain constant modulus waveforms. When a constellation $\mathcal{J}$ of cardinality $|\mathcal{J}| = J$ is utilized, $\beta = M_T^c \log_2 J + \lfloor \log_2 \binom{M}{M_T^c} \rfloor$ uncoded bits are conveyed in each GSM symbol. Compared with fixed antenna allocation approaches with the same constellation order, GSM enables $\lfloor \log_2 \binom{M}{M_T^c} \rfloor$ additional bits to be embedded in each symbol. The transmission does not require knowledge of the underlying communication channel. When such CSI is available, it can be exploited by, e.g., spatial precoding [31].

An example of GSM transmission is shown in Fig. 3. In this example, the antenna array has $M = 4$ elements. A single antenna is used for each symbol, i.e., $M_T^c = 1$ and $\lfloor \log_2 \binom{4}{1} \rfloor = 2$ bits are embedded in the combination of transmit antennas. A binary phase shift keying (BPSK) modulation is utilized, thus $\mathcal{J} = \{\pm 1\}$, $J = 2$, and a total of $R = 3$ bits are conveyed in each symbol. In the example in Fig. 3, the message 101 is divided into spatial selection bits 10 and constellation bit 1. According to the element mapping rule, antenna A2 transmits the BPSK symbol $+1$.

In GSM signalling, only a subset of the antenna array is used, and the transmit elements change between different symbols. Hence, the remaining elements can be assigned to radar transmission, leading to the proposed GSM-based DFRC system, which complies with the constraints discussed in Section II-A. As each radar pulse consists of $K$ symbol slots, a total of $K \cdot R$ bits are conveyed in each PRI.

*2) Communications Receiver Operation:* To formulate how the transmitted signal is decoded by the receiver, we first model the channel output. In the following we consider a MIMO receiver with $M_R^c$ antennas, which has full CSI.

Since radar and communications use distinct bands, no cross interference exists. Consequently, by letting $\mathbf{x} \in \mathcal{X} \subset (\mathcal{J} \cup \{0\})^M$ denote the channel input at the communication frequency range, it holds that $\mathbf{x}$ is sparse with support size $M_T^c$, i.e., $\mathcal{X}$ is the set of $M_T^c$ sparse vectors in $(\mathcal{J} \cup \{0\})^M$. Therefore, assuming a linear memoryless channel $\mathbf{H} \in \mathbb{C}^{M_R^c \times M}$ whose output is corrupted by an additive noise vector $\mathbf{w}^{(c)} \in \mathbb{C}^{M_R^c}$, the channel output representing a single GSM symbol observed by the receiver, denoted as $\mathbf{y}^{(c)} \in \mathbb{C}^{M_R^c}$, is given by $\mathbf{y}^{(c)} = \mathbf{H}\mathbf{x} + \mathbf{w}^{(c)}$. The received signal is directly processed without using dedicated pre-processing. Since the receiver has full CSI, i.e., knowledge of the matrix $\mathbf{H}$ and the distribution of $\mathbf{w}^{(c)}$, it can decode with minimal probability of error using the maximum a-posteriori probability rule. Assuming that the data bits are equiprobable, this symbol detection rule is given by

$$\hat{\mathbf{x}} = \arg\max_{\mathbf{x} \in \mathcal{X}} p\left(\mathbf{y}^{(c)} | \mathbf{x}, \mathbf{H}\right). \tag{1}$$

For example, when the noise obeys a white Gaussian distribution, (1) specializes to the minimum distance detector.

Given the detected $\hat{\mathbf{x}}$, the spatial selection bits can then be recovered from the support of $\hat{\mathbf{x}}$, while the constellation bits are demodulated from its non-zero entries. Recovering $\hat{\mathbf{x}}$ via (1) generally involves searching over the set $\mathcal{X}$ whose cardinality is $2^\beta$. When specialized to the minimum distance detector, e.g., when the conditional distribution in (1) is Gaussian, the complexity is of the order of $\mathcal{O}(2^\beta M_T^c M_R^c)$ products, as evaluating the distance for each tested $\mathbf{x} \in \mathcal{X}$ involves $M_T^c M_R^c$ multiplications. This implies that the computational complexity grows with the dimensionality of the system, i.e., the number of antenna elements, as well as with the cardinality of the search space. Nonetheless, when $\beta$ is large, one can implement symbol detection with lower computational burden using existing reduced complexity GSM decoding methods, see e.g., [15]. Doing so allows SpaCoR to be utilized with controllable decoding complexity at the receiver side, at the cost of some performance degradation. In our experimental study detailed in Section VI we consider scenarios in which $\beta$ is relatively small, and thus carry out symbol detection by directly computing (1).

*D. Radar Subsystem*

To formulate the radar subsystem, in the following we first model its transmitted and received signal, after which we introduce an algorithm for radar detection.

SpaCoR uses a phased array radar, which enables to steer the radar beam at the direction of interest. Such beam steering is achieved by using a single waveform, denoted by $s(t)$, while assigning a different weight per each element designed to steer the beam in a desired direction $\theta_T$. The transmit power is denoted as $P_t := \frac{1}{T_{\mathrm{PRI}}} \int_0^{T_{\mathrm{PRI}}} |s(t)|^2 dt$, where $T_{\mathrm{PRI}}$ is the pulse repetition interval. For a ULA with $M$ elements, the weight function of the $m$th element is $a_m(\theta_T) = e^{-j\frac{2\pi m d \sin \theta_T}{\lambda}}$, where $\lambda$ is the wavelength, and the corresponding waveform is $s_m(t) = s(t) a_m(\theta_T)$. For a narrowband waveform, the signal received in the far field at angle $\theta$ and range $\xi$ is expressed as [32, Ch. 8.2]

$$y_\theta^{(r)}(t) = s\left(t - \frac{\xi}{c}\right) \sum_{m=0}^{M-1} a_m(\theta_T) a_m^*(\theta), \tag{2}$$

where $a_m^*(\theta)$ is the steering weight between the $m$th element and the far field target at angle $\theta$, and $c$ is the speed of light.

Unlike traditional phased array radar, which utilizes the complete antenna array, SpaCoR assigns only a subset of the antenna elements for radar signalling at each time instance, and the antenna allocation pattern dynamically changes between different communication symbols. In particular, letting $T_c$ be the duration of a communication symbol, each radar pulse consists of $K$ consecutive communication symbols, i.e., the pulse width is $T_r = K T_c$. At each time slot, $M_r^r = M - M_T^c$ antenna elements are assigned for radar transmission. Let $m_{k,0} < m_{k,1} < \cdots < m_{k,l} \cdots < m_{k,M_T^r - 1}$ be random variables representing the element indices assigned to radar at the $k$th time slot, where $m_{k,l} \in \{0, 1, \ldots, M-1\}$ for each $k, l$. For instance, in the illustration in Fig. 2(c), the antenna indices assigned to radar at the 0th time slot of the first pulse are 1 and 3, and thus $m_{0,0} = 1$ and $m_{0,1} = 3$. The received signal of the proposed scheme, which for conventional phased array is given by (2), is

expressed as

$$y_\theta^{(r)}(t) = s\left(t - \frac{\xi}{c}\right) \sum_{k=0}^{K-1} g\left(\frac{t - kT_c - \frac{\xi}{c}}{T_c}\right) \tilde{\rho}_T(k, \theta), \quad (3)$$

where $g(t)$ is a rectangular window of unity support, and $\tilde{\rho}_T(k, \theta) := \sum_{l=0}^{M_T^r - 1} a_{m_{k,l}}(\theta_T) \cdot a_{m_{k,l}}^*(\theta)$ is the transmit gain at the $k$th time slot. Denote $\vartheta := \frac{2\pi d \sin\theta}{\lambda}$ and $\vartheta_T := \frac{2\pi d \sin\theta_T}{\lambda}$ as the spatial frequencies at the direction of radar target and the direction of the transmit beam, respectively. The transmit beam pattern $\tilde{\rho}_T(k, \theta)$ can be rewritten as

$$\tilde{\rho}_T(k, \vartheta) = \sum_{l=0}^{M_T^r - 1} e^{j m_{k,l}(\vartheta - \vartheta_T)}. \quad (4)$$

The time delay experienced by the echoes reflected from the radar target until reaching the $m$th receive antenna element is $\frac{\xi}{c} - \frac{m\vartheta}{2\pi}$. After frequency down conversion by mixing with the local carrier, the echo received in the $m$th antenna element can be expressed as

$$y_m^{(r)}(t) = \alpha y_\theta^{(r)}\left(t - \frac{\xi}{c} + \frac{m\vartheta}{2\pi}\right) e^{-j2\pi f_c t} + w_m^{(r)}(t), \quad (5)$$

where $\alpha$ is the reflective factor of the target, $w_m^{(r)}(t)$ is the noise at the $m$th antenna receiver, modeled as a white Gaussian process. Let $h(t)$ be the baseband radar waveform and $f_c$ denote the carrier frequency, i.e., $s(t) = h(t)e^{j2\pi f_c t}$. With the narrowband assumption, i.e., $\frac{Md}{c} \ll \frac{1}{B_r}$, where $B_r$ is the bandwidth of the radar waveform, one can use the approximation $y_\theta^{(r)}(t - \frac{\xi}{c} + \frac{m\vartheta}{2\pi}) \approx y_\theta^{(r)}(t - \frac{\xi}{c}) e^{j m\vartheta}$. Substituting (3) into (5), and defining the round trip delay $\tau := 2\xi/c$, it follows that

$$y_m^{(r)}(t) = \alpha h_m(t, \tau, \vartheta) + w_m^{(r)}(t), \quad (6)$$

where

$$h_m(t, \tau, \vartheta) := e^{-j2\pi f_c \tau + j m\vartheta}$$
$$\times \sum_{k=0}^{K-1} \tilde{\rho}_T(k, \vartheta) g\left(\frac{t - kT_c - \tau}{T_c}\right) h(t - \tau). \quad (7)$$

The radar ehco is received at the idle time of the pulse, the duration of which is $T_{\text{rec}} := T_{\text{PRI}} - T_r$. The received signal is uniformly sampled with Nyquist rate $F_s$, i.e., $F_s \geq B_r$. While it is possible to sample below the Nyquist rate by using generalized sampling methods as was done in [33], [34], we leave the study of SpaCoR with sub-Nyquist sampling for future work. The number of sample points in each PRI is $N_{\text{rec}} = \lfloor \frac{T_{\text{rec}}}{T_s} \rfloor$, and the sample time instances are $t = nT_s$, where $n \in \{0, 1, \ldots, N_{\text{rec}} - 1\}$. By defining $h_m[n, \tau, \vartheta] := h_m(nT_s, \tau, \vartheta)$, and $w_m^{(r)}[n] := w_m^{(r)}(nT_s)$, the sampled signal vector (6) is given by

$$y_m^{(r)}[n] := \alpha h_m[n, \tau, \vartheta] + n_m^{(r)}[n]. \quad (8)$$

The discrete-time model in (8) can be extended to a scenario with multiple targets. Let $L$ be the number of targets, and denote the reflective factor, the spatial frequency, and the delay of the $l$th target by $\alpha_l$, $\vartheta_l$, and $\tau_l$, respectively. The reflected echoes

from multiple targets are expressed as

$$y_m^{(r)}[n] = \sum_{l=0}^{L-1} \alpha_l h_m[n, \tau_l, \vartheta_l] + w_m^{(r)}[n]. \quad (9)$$

In radar detection, the task is to recover the target parameters $\{\tau_l, \vartheta_l, \alpha_l\}_{l=0}^{L-1}$ from the received signal in (9).

*1) Radar Detection:* The SpaCoR radar receiver estimates the parameters $\{\tau_l, \vartheta_l, \alpha_l\}_{l=0}^{L-1}$ using sparse recovery methods. To formulate the radar detection scheme, we consider the case in which the target delay $\tau$ satisfies $\tau \in [\tau_{\min}, \tau_{\max})$, where $\tau_{\min}$ and $\tau_{\max}$ are a-priori known minimal and maximal delays, respectively. To recover the parameters of the targets, we divide the range of target delay into a grid of $P$ uniformly-spaced points with an interval $\delta\tau \leq \frac{1}{B_r}$, where $B_r$ is the bandwidth of the radar waveform. Similarly, the spatial frequency range $\vartheta \in [-\pi, \pi)$ is divided into $Q$ equally-spaced points with an interval $\delta\vartheta \leq \frac{2\pi}{M}$. The grid sets of the discretized delay and spatial frequency are denoted as $\mathcal{D} := \{\tau^p = \tau_{\min} + \frac{p}{P}(\tau_{\max} - \tau_{\min}) | p = 0, 1, \ldots, P - 1\}$, and $\Theta := \{\vartheta^q = -\pi + 2\pi\frac{q}{Q} | q = 0, 1, \ldots, Q - 1\}$, respectively. Assuming that the targets are located on the discretized grids, the echoes in (9) can be written as

$$\mathbf{y}^{(r)} = \mathbf{A}\mathbf{b} + \mathbf{w}^{(r)}, \quad (10)$$

where $\mathbf{y}^{(r)} \in \mathcal{C}^{N_{\text{rec}}M}$ is the received sample vector whose entries are $[\mathbf{y}^{(r)}]_{mN_{\text{rec}}+n} := y_m^{(r)}[n]$; $\mathbf{A}$ is the observation matrix, the entries of which are given by

$$[\mathbf{A}]_{mN_{\text{rec}}+n, pQ+q} := h_m[n, \tau^p, \vartheta^q], \quad (11)$$

and $\mathbf{b} \in \mathcal{C}^{PQ}$ is a vector with $L$ nonzero entries encapsulating the parameters of the targets. The $(pQ + q)$th entry of $\mathbf{b}$ equals $\alpha_l$ if $\tau^p = \tau_l$ and $\vartheta^p = \vartheta_l$, while the other entries equal 0. Here, we assume $\mathbf{b}$ is sparse, i.e., $L \ll PQ$. The vector $\mathbf{w}^{(r)}$ is a zero mean white Gaussian noise vector, obtained by $[\mathbf{w}^{(r)}]_{mN_{\text{rec}}+n} := \mathbf{w}_m^{(r)}[n]$, with variance $\sigma_r^2$.

Due to the sparsity of $\mathbf{b}$, it can be recovered by solving

$$\min_{\mathbf{b}} \|\mathbf{b}\|_0, \text{ subject to } \|\mathbf{y}^{(r)} - \mathbf{A}\mathbf{b}\|_2 \leq \epsilon, \quad (12)$$

where $\epsilon$ is related to the noise level. The optimization problem (12) can be solved by compressed sensing (CS) algorithms, such as greedy approaches, $l_1$ norm optimization, and other sparse recovery schemes, as detailed in [35], [36]. The computational complexity of solving (12) depends on the chosen CS algorithm. While the detailed complexity analysis is out of the scope of the current paper, we quantify the computational complexity of this task by considering orthogonal matching pursuit (OMP) algorithm, which belongs to the family of greedy approaches, and has a complexity order of $\mathcal{O}(LPQN_{\text{rec}})$ [37]. This complexity order indicates that, for a given number of targets and received samples, the complexity grows with the density of the grids via $P$ and/or $Q$. Consequently, as finer grids imply higher accuracy, one can trade computational complexity for recovery accuracy.

## III. PERFORMANCE ANALYSIS OF THE RADAR SUBSYSTEM

We now study the performance of SpaCoR, which consists of radar and communication subsystems. The latter implements conventional GSM signaling, whose performance has already been analyzed in the communication literature, e.g., [28], [30].

Therefore, in the following we only provide the analysis of the radar subsystem, characterizing how it is affected by the incorporation of GSM signalling as a DFRC system. The performance measures of the communication subsystem are evaluated through simulation in Section VI-B.

To analyze the performance of radar subsystem, we focus our analysis on the two-dimensional delay-direction transmit beam pattern, defined as the correlation between the echoes from the steered beam direction and the echoes from the target direction. This measure can be used to characterize the radar resolution and the mutual interference between multiple targets [38].

As the spatial allocation pattern of the transmit array in SpaCoR is determined by the transmitted message, the transmit beam pattern of its radar subsystem varies between different communication symbols, thus we compute it by taking the correlation over all symbols transmitted within a single pulse. In particular, we first characterize the delay-direction transmit beam pattern which arises from the received signal model. Then, we study it statistical properties and compare them to those achieved when using the complete antenna array, as well as with fixed antenna allocation.

## A. Transmit Beam Pattern

In the following we characterize the transmit beam pattern of the radar subsystem. Without loss of generality, we express the transmit beam pattern by focusing on the echo captured in a single receive antenna, and particularly on that of index $m = 0$. To properly define the transmit beam pattern, we assume that a target with unit reflective factor is located at $(\tau, \vartheta)$. The noiseless echo at received antenna $m = 0$, i.e., when the noise term in (5) is nullified, is given by $y_0^{(r)}[n, \tau, \vartheta] := h_0[n, \tau, \vartheta]$. Similarly, the echo of the reference target, which is with unit reflective and located in $(\tilde{\tau}, \vartheta_T)$ is given by $y_0^{(r)}[n, \tilde{\tau}, \vartheta_T]$. The transmit delay-direction beam pattern is defined as the correlation of $y_0^{(r)}[n, \tau, \vartheta]$ and $y_0^{(r)}[n, \tilde{\tau}, \vartheta_T]$, i.e., $\chi_T(\tau, \vartheta) := \sum_{n=0}^{N_{\text{rec}}-1} h_0[n, \tau, \vartheta] h_0^*[n, \tilde{\tau}, \vartheta_T]$. By substituting (7) into the definition of $\chi_T(\tau, \vartheta)$, we obtain

$$\chi_T(\tau, \vartheta) = e^{-j2\pi f_c(\tau-\tilde{\tau})} \sum_{n=0}^{N_{\text{rec}}-1} \sum_{k=0}^{K-1} \tilde{\rho}_T(k, \vartheta)$$

$$\times g\left(\frac{nT_s - kT_c - \tau}{T_c}\right) h[n, \tau] h^*[n, \tilde{\tau}]. \quad (13)$$

The summation over $n = 0, \ldots N_{\text{rec}} - 1$ in (13) represents the averaging of the correlation over the entire radar pulse.

As the phase term $e^{-j2\pi f_c(\tau-\tilde{\tau})}$ in (13) disappears by taking the absolute value, it does not affect the magnitude of the transmit beam pattern. Hence, the term $e^{-j2\pi f_c(\tau-\tilde{\tau})}$ is omitted in the sequel, and (13) is rewritten as

$$\chi_T(\tau_d, f_\theta) = \sum_{n=0}^{N_{\text{rec}}-1} \sum_{k=0}^{K-1} \rho_T(k, f_\theta) g\left(\frac{nT_s - kT_c - \tau_d - \tilde{\tau}}{T_c}\right)$$

$$\times h[n, \tau_d + \tilde{\tau}] h^*[n, \tilde{\tau}], \quad (14)$$

where $\tau_d := \tau - \tilde{\tau}$ is the delay difference, $f_\theta := \vartheta - \vartheta_T$ is the difference in the spatial frequency, and $\rho_T(k, f_\theta) := \tilde{\rho}_T(k, \vartheta)$. Since the antenna indices $\{m_{k,l}\}$, which are encapsulated in $\tilde{\rho}_T(\cdot, \cdot)$ by (4), are random, it holds that $\chi_T(\tau_d, f_\theta)$ in (14) is
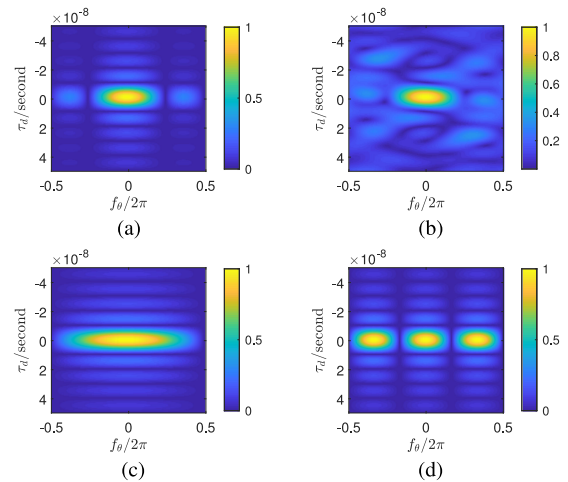


Fig. 4. Normalized transmit beam patterns of the analyzed schemes. In this illustration, the parameter are set following Table I.

random. In the following, we analyze the beam pattern of SpaCoR compared to using the complete array for radar signaling, as well as to using fixed subsets.

## B. Comparison of Different Antenna Allocation Schemes

We begin with the transmit beam pattern achieved when utilizing the full antenna array for radar transmission, used as a basis for comparison. Then, the beam patterns of SpaCoR as well as fixed antenna allocation methods are evaluated.

We henceforth focus on radar signalling with chirp waveforms. Here, the baseband radar waveform $h(t)$ is

$$h(t) = g\left(\frac{t}{T_r}\right) \exp\left\{j\mu\pi\left(t - \frac{T_r}{2}\right)^2\right\}, \quad (15)$$

where $\mu$ is referred to as the frequency modulation rate. The bandwidth of the chirp is defined as $B_r := \mu T_r$.

*1) Full Antenna Array:* When the full antenna array is used, the transmit beam pattern can be obtained as a special case of (14) by setting $M_T^{(r)} = M$. Hence, the antenna indices are deterministic and are given by $m_{k,l} = l$ for each $k = 0, 1, \ldots, K - 1$. The resulting transmit delay-direction beam pattern is a deterministic quantity.

The full array transmit beam pattern, obtained by substituting (15) and $M_T^{(r)} = M$ into (14), is [39, Ch. 3A]

$$\left|\chi_T^{\text{Full}}(\tau_d, f_\theta)\right| = N_r \left|\text{sinc}(B_r\tau_d)\right| \cdot \left|\frac{\sin(M f_\theta/2)}{\sin(f_\theta/2)}\right|, \quad (16)$$

where $N_r := \lfloor T_r/T_s \rfloor$. The normalized transmit beam pattern for the full antenna array is depicted in Fig. 4(a). In this beam pattern, the peak located in $\tau_d = 0$ and $f_\theta = 0$ is denoted as the mainlobe and the other peaks are denoted as the sidelobes. The width of the mainlobe determines the resolution of the radar system, while the sidelobes influence the interference induced by clutters in the environment and the coupling between nearby targets.

*2) SpaCoR:* In SpaCoR, for a given time slot $k$, different indices of the radar transmitting antennas $\{m_{k,l}\}$ are selected. As the switching of transmit antennas is determined by the random communication data stream, the transmit beam pattern is a random quantity. The usage of stochastic beam patterns due to

random array configuration is an established concept in the radar literature, see, e.g., [40]. In particular, the following analysis extends the study of delay-direction beam patterns due to the randomized switch antenna array with a single active element, investigated in [38], to multiple active elements.

We analyze the statistical moments of the beam pattern, which provide means for evaluating the resolution and the sidelobe level of SpaCoR. In particular, we show that the expected beam pattern of SpaCoR, which is approached by the averaged beam pattern over a large number of pulses, is identical to that of the full antenna array up to a constant factor. This holds due to the following theorem:

*Theorem 1:* The absolute value of the expected transmit delay-direction beam pattern (14) of SpaCoR is

$$\left| \mathcal{E} \left\{ \chi_T^{\mathrm{GSM}} \left( \tau_d, f_\theta \right) \right\} \right| \\ = \frac{M_T^r}{M} \left| \sum_{n=0}^{N_{\mathrm{rec}}-1} h \left[ n, \tau_d + \tilde{\tau} \right] h^* \left[ n, \tilde{\tau} \right] \right| \cdot \left| \frac{\sin \left( M f_\theta / 2 \right)}{\sin \left( f_\theta / 2 \right)} \right|. \quad (17)$$

*Proof:* The proof is given in Appendix A. ∎

The expectation in (17) is carried out with respect to the random antenna indices $\{m_{k,l}\}$. These indices are determined by the communicated bits, which are assumed to be i.i.d. It follows from the law of large number that as the number of pulses grows, the average transmit beam pattern approaches its expected value with probability one [41, Ch. 8.4]. Consequently, in the large number of pulses horizon, the magnitude of the average transmit beam pattern coincides with (17).

Theorem 1 is formulated for arbitrary waveforms $h(t)$. For chirp signals, it is specialized in the following corollary:

*Corollary 1:* The absolute value of the expected transmit beam pattern (14) for SpaCoR with chirp waveform is

$$\left| \mathcal{E} \left\{ \chi_T^{\mathrm{GSM}} \left( \tau_d, f_\theta \right) \right\} \right| = \frac{M_T^r N_r}{M} \left| \mathrm{sinc} \left( B_r \tau_d \right) \right| \cdot \left| \frac{\sin \left( M f_\theta / 2 \right)}{\sin \left( f_\theta / 2 \right)} \right|. \quad (18)$$

*Proof:* The corollary is obtained by substituting (15) into the expected transmit beam pattern in (17). ∎

Corollary 1 implies that SpaCoR, which utilizes the antenna array for both radar signalling and communication transmission without using multiband signals, has the same expected beam pattern as in (16) (up to a constant factor), i.e., the same as when using the complete array only for radar. This implies that, e.g., when averaged over a large number of pulses, SpaCoR achieves the same ratio of the sidelobe level to the mainlobe as that of using the complete array for radar.

For a single radar pulse with a finite number of symbols, the difference between the (random) instantaneous transmit beam pattern and its expected value is dictated by its variance [41, Ch. 5]. Consequently, larger variance induces increased fluctuations in the transmit beam patterns compared to its expected value (18). The variance of the transmit beam pattern with chirp waveforms is stated in the following proposition:

*Proposition 1:* The variance of the normalized transmit delay-direction beam pattern (14) with chirp waveform (15) is

$$\mathcal{V} \left\{ \chi_T^{\mathrm{GSM}} \left( \tau_d, f_\theta \right) / \mathcal{E} \left\{ \chi_T^{\mathrm{GSM}} (0,0) \right\} \right\} = \gamma^{\mathrm{GSM}} \left( \tau_d \right) \\ \times \left[ \frac{\left( M_T^r - M \right)}{M_T^r M^2 \left( M - 1 \right)} \cdot \left| \frac{\sin \left( M f_\theta / 2 \right)}{\sin \left( f_\theta / 2 \right)} \right|^2 + \frac{\left( M - M_T^r \right)}{M_T^r \left( M - 1 \right)} \right],$$

where

$$\gamma^{\mathrm{GSM}} \left( \tau_d \right) := \frac{\mathrm{sinc}^2 \left( B_r \tau_d / K \right)}{K} = \frac{\mathrm{sinc}^2 \left( \mu T_c \tau_d \right)}{K}. \quad (19)$$

*Proof:* The proof is given in Appendix B. ∎

From Proposition 1 it follows that the variance decreases when $K$ increases. A small variance leads to an improved beam pattern, as it is less likely to deviate from its desired mean value when the variance of the beam pattern decreases.

The similarity between the beam patterns of SpaCoR and that of using the full array is demonstrated in Fig. 4. In particular, Fig. 4(b) is a realization of the average beam pattern in a single pulse of SpaCoR with $K = 12$ symbols and $M_T^{(r)} = 2$ antennas assigned for radar, while Fig. 4(a) is the corresponding beam pattern when using all the $M = 4$ elements for radar. Comparing Fig. 4(a) and Fig. 4(b) shows the similarity of the beam pattern of SpaCoR, in terms of mainlobe width and sidelobe levels, to that achieved when using the full antenna array for radar.

*3) Fix1 Scheme:* In this scheme, the full antenna array is divided into two sub-ULAs, one for radar and one for communication, in a fixed manner. The indices of the transmit elements are $m_{k,l} = l$ for each $k$, as when using the full array for radar signalling. However, here only a subset of the array is used for radar, i.e., $M_T^{(r)} < M$. The resulting deterministic transmit beam pattern is stated in the following proposition:

*Proposition 2:* The transmit beam pattern of *Fix1* with chirp waveforms is given by

$$\left| \chi_T^{\mathrm{Fix1}} \left( \tau_d, f_\theta \right) \right| = \frac{M_T^r N_r}{M} \left| \mathrm{sinc} \left( B_r \tau_d \right) \right| \cdot \left| \frac{\sin \left( M_T^r f_\theta / 2 \right)}{\sin \left( f_\theta / 2 \right)} \right|. \quad (20)$$

*Proof:* The proposition is obtained by substituting the transmit antenna indices $m_{k,l} = l$ and (15) into (14). ∎

As $M_T^r < M$, the mainlobe in (20) is wider then that of (16). The normalized transmit beam pattern of *Fix1* is depicted in Fig. 4(c), which is computed using the same settings as in Figs. 4(a)–4(b), where it is indeed observed that its mainlobe is wider than that of the full antenna array.

*4) Fix2 Scheme:* An alternative allocation approach is to randomly divide the antenna array into two sub-arrays: One for radar and the other for communications. In this method, the indices of the transmit elements are randomized and remain unchanged during the whole radar pulse duration, i.e., $\{m_{k,l}\}$ is the same set of random variables for each $k = 0, 1, \ldots, K - 1$. A realization of the normalized transmit beam pattern for *Fix2* is depicted in Fig. 4(d). When we only consider the radar subsystem, this approach can be regarded as a specific case of SpaCoR by setting $K = 1$, and the expected value and variance of the transmit delay-direction beam pattern are obtained by substituting $K = 1$ into (17) and (19), respectively. As the parameter $K$ does not affect the expectation of the transmit beam pattern (18), it holds that the expected transmit delay-direction beam pattern of *Fix2* is the same as that of SpaCoR. However *Fix2* has a higher sidelobe level compared with SpaCoR, which can be evaluated through its variance, as stated in the following corollary:

*Corollary 2:* The variance of the normalized transmit delay-direction beam pattern with chirp waveform is written as

$$\mathcal{V} \left\{ \chi_T^{\mathrm{Fix2}} \left( \tau_d, f_\theta \right) / \mathcal{E} \left\{ \chi_T^{\mathrm{Fix2}} (0,0) \right\} \right\} = \gamma^{\mathrm{Fix2}} \left( \tau_d \right) \\ \times \left[ \frac{\left( M_T^r - M \right)}{M_T^r M^2 \left( M - 1 \right)} \cdot \left| \frac{\sin \left( M f_\theta / 2 \right)}{\sin \left( f_\theta / 2 \right)} \right|^2 + \frac{\left( M - M_T^r \right)}{M_T^r \left( M - 1 \right)} \right], \quad (21)$$

where

$$\gamma^{\text{Fix2}}(\tau_d) := \text{sinc}^2(B_r \tau_d). \tag{22}$$

*Proof:* Setting $K = 1$ in Proposition 1 proves (21). ∎

Comparing (19) with (22), we find that for a given pulse width $T_r$, the maximal variance of the transmit beam pattern for *Fix2*, i.e., (22) for $\tau_d = 0$, is $K$ times that of SpaCoR. This demonstrates that the dynamic changing of antenna elements, whose purpose in SpaCoR is to increase the communications rate, allowing to convey more GSM symbols in each radar pulse, also improves the radar angular resolution and decreases the sidelobe levels. The performance advantages of SpaCoR over the fixed antenna allocation approaches are numerically observed in Section VI.

## IV. Hardware Prototype High Level Design

To demonstrate the feasibility of the proposed DFRC system, we implemented SpaCoR using a dedicated hardware prototype. This prototype, used here to experiment SpaCoR, can realize a multitude of DFRC systems, as it allows baseband waveform generation, over-the-air signaling, frequency band waveform transmission, radar echo generation, radar echo reception, and communication signal reception. In this section, we describe the high level design of the prototype, detailing the structure of each component in Section V. The overall system structure is described in Section IV-A, and in Section IV-B, we introduce how to choose the system parameters. Finally, in Section IV-C we present how the joint radar and communications (JRC) waveforms transmitted by each antenna element are generated in the prototype.

### A. Overall System Architecture

The overall structure of the prototype and the high level information flow of the experimental setup are depicted in Fig. 5. Our setup consists of 1) a PC server, which provides graphical user interface (GUI) for setting the DFRC parameters, generates the waveforms, and processes the received signals; 2) a two-dimensional digital antenna array with 16 elements, which enables to independently control each element. In our experiment, the array is divided into 8 transmit elements and 8 receive elements; 3) a pair of field-programmable gate array (FPGA) boards interfacing the DFRC transmitted and received signals, respectively, between the PC and the antenna; and 4) a radar echo generator (REG) which receives the transmitted waveform and generates the reflected echoes.

Through the GUI, the parameters of the radar and communication subsystems, as well as those of the experimental setup, are configured. Once the paramerers are set and an experiment is launched, the JRC waveform is generated by the PC application. Then, the JRC waveform is transferred to the DFRC transmit FPGA in which it is converted into analog, up-converted to passband, and forwarded to the DFRC antenna array for transmission. The transmitted waveform is received by the REG, which in response transmits echoes simulating the presence of radar targets, as well as by a receive antenna, which is connected to the receive FPGA. The received radar echoes at the DFRC antenna and the received communications signal are down-converted, digitized and then sent to the PC server. The digitized signals are processed by the PC application, which in turn recovers the radar targets and the communication messages.
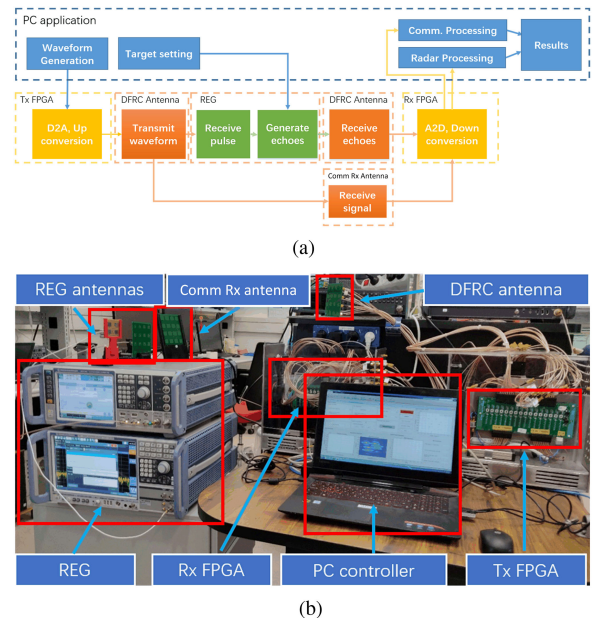


Fig. 5.  The high level structure and components of the DFRC prototype. (a) Experimental setup flow diagram. (b) DFRC prototype.

### B. System Parameterization

In order to guarantee the performances of both radar and communications systems, several criteria should be considered when designing the system parameters. The design of radar waveform parameters, including PRI, radar bandwidth, pulse width, etc., have been well studied and can be found in [32], [42]. Here, we discuss how to choose the parameters unique to the proposed DFRC system, i.e., $M_T^r$, $M_T^c$ and $K$.

*1) Number of Elements Allocated for Radar:* For the radar subsystem, which is considered to be the primary functionality, the maximal detection range is related to the antenna transmit gain, which approximately equals $(M_T^r)^2 P_t$. Hence, the minimum number of antenna elements should satisfy the requirement of radar detection range and can be determined according to the radar equation [32, Ch. 2]. Once $M_T^r$ is determined, the value of $M_T^c$ is obtained as $M_T^c = M - M_T^r$.

*2) Number of Chips Per Pulse:* An additional unique parameter of SpaCoR is the number of chips per each radar pulse, denoted $K$. The implementation of SpaCoR involves RF switches which allow each antenna element to toggle between radar and communication signalling multiple times within a pulse. When the duration of the radar pulse width is fixed, the number of chips, i.e., communications symbols, is dictated by the switching speed of these devices, as the duration of each chip should be sufficiently larger than this switching time to allow the communication symbols to be fully transmitted. Consequently, the main consideration in setting $K$ is the overhead dictated by the switching speed of the RF switches. Moreover, the setting of $K$ must also account for the radar and communication bands. Based on the radar performance analysis presented in Section III, the variance of the transmit beam pattern decreases when $K$ increases. This indicates that larger values of $K$ are preferable. Furthermore, for the radar subsystem, the chirp is divided into $K$ short chips. The bandwidth with a rectangular window function of duration $T_r/K = T_c$ is $1/Tc$, which is the bandwidth of
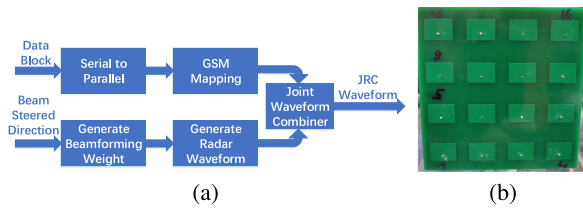
Fig. 6. Waveform generator block diagram (left) and antenna array (right).



Fig. 7. FPGA board, DAC card Radio frequency card of the transmitter.

the communications signal. If $1/T_c$ is larger than $B_r/K$, the bandwidth of a short chirp chip will be expanded in frequency spectrum. Thus, we require $B_r/K > 1/T_c = K/T_r$, i.e, $K^2 < B_r T_r$. Finally, the communication channel is assumed to be flat, requiring the bandwidth of the communications signal to be smaller than the coherence bandwidth, i.e., $1/T_c < B_c$, where $B_c$ is the coherence bandwidth of the communication channel. Thus, the value of $K$ should be set to $K < \min\{\sqrt{B_r T_r}, T_r B_c\}$. To summarize, in light of the aforementioned considerations, the number of chips per pulse should account for both the hardware complexity as well as the system performance.

### C. Generation of the JRC Waveform

As detailed in Section II, our system implements radar and communications by allocating different antenna elements to each functionality in a randomized fashion. Unlike traditional GSM communications in which the active antenna are changed using switching [43], our prototype embeds the randomized allocation pattern into a dedicated JRC waveform. Here, we describe how these joint waveforms are generated.

A block diagram of the JRC waveform generator is depicted in Fig. 6(a): The inputs of the generator are the communication data block and the steered direction of the radar beam. The output of the waveform generator is the JRC waveform for each antenna element. The JRC waveform transmitted determines the allocation pattern of the antenna array. The generation process consists of the following steps:

1) Communication symbol generator: the conversion of the data block into GSM symbols consists of two modules:
   - Serial-to-parallel (S/P) module, where the data block is divided into multiple GSM blocks. Each GSM block consists of two sets of bits: spatial selection bits, used for determining the antenna allocation, and constellation bits, conveyed in the communication symbol.
   - GSM mapping module, which maps each GSM block into its corresponding constellation symbol and antenna allocation pattern.
2) Radar waveform generator: the beam direction is converted into a radar waveform via the following modules:
   - Beamforming weight generation, which assigns the weights to direct towards the steered direction.
   - Radar waveform generation, which weights the initial radar waveform to obtain the desired beampattern.
3) Radar and communications waveform combiner: the JRC waveform is generated by combining the radar waveform and communication symbol blocks. In this combiner, the communication chips are inserted into the radar waveform based on the antenna allocation bits. An example for such a combined waveform is depicted in Fig. 2(c).

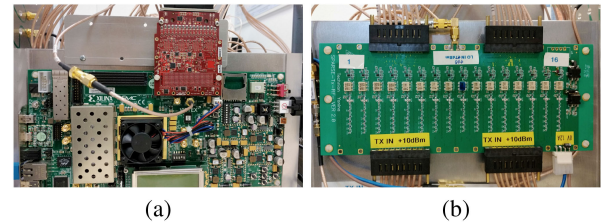As illustrated in Fig. 2(c), the JRC waveform is divided into multiple time slots, where the length of each slot is dictated by the communication symbol duration. In each time slot, the allocation of the array element is determined by the content of its waveform. This joint waveform generation process facilitates the application of SpaCoR without utilizing complex high speed switching devices.

## V. PROTOTYPE REALIZATION

In the previous section, we introduced the design philosophy of the DFRC prototype, which divides the implementation of our scheme between software and dedicated hardware components. The prototype is depicted in Fig. 5(b): It consists of a PC server, a DFRC Tx board, a DFRC Rx board, a REG, and a two dimensional antenna array with 16 elements. The GUI and data processor are implemented in software on the PC server. In this section we present the structure of each component in our DFRC prototype, detailing the hardware and software modules in Sections V-A–V-B, respectively.

### A. Hardware Components

*1) Antenna Array:* A two dimensional patch antenna array with 16 elements is used in our prototype, depicted in Fig. 6(b). The antenna works with carrier frequency 5.1 GHz and has a 80 MHz bandwidth. The size of each patch is 1.8 cm × 1.3 cm. The horizontal distance and the vertical distance between two horizontally adjacent elements and two vertically adjacent elements are 2.7 cm and 2.7 cm, respectively. Rather than implementing the transmit array and receive array in a time-division manner, we utilize 8 elements for transmission and 8 elements for receive, which avoids using the duplexers thus decreases the hardware complexity. Since the received signal models are the same for both hardware realizations, the resulting prototype complies with our description and analysis of SpaCoR.

*2) DFRC Tx Board:* The input of the transmitter is a set of 8 digital JRC waveforms generated by the PC server, each intended for a different element. In the transmitter, the digital JRC waveform is converted into analog, up-converted to passband, and amplified. The resulting analog waveform is forwarded to the transmit antenna using 8 cables.

This process is implemented using three components: An FPGA board, a digital-to-analog convertor (DAC) card, and an up-conversion card. These components are depicted in Fig. 7. High speed data transmission interface is realized on the FPGA, which transfers the digital waveform data from the portable server to the DAC board. Each of the 8 digital signals is converted to analog using a 4DSP FMC216 DAC card. The FMC216 provides sixteen 16-bit DAC at 312.5 Msps (interpolated to 2.5 Gsps) based on TI DAC39J84 chip. In the up-conversion card, the analog waveform is up-converted using a local oscillator and amplified by a passband filter. After digital to analog conversion
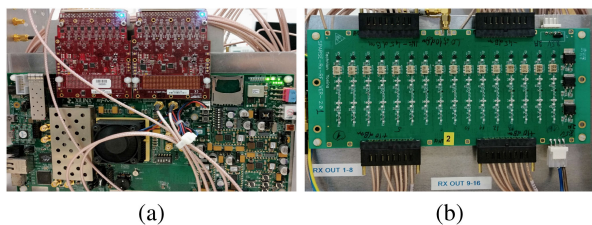
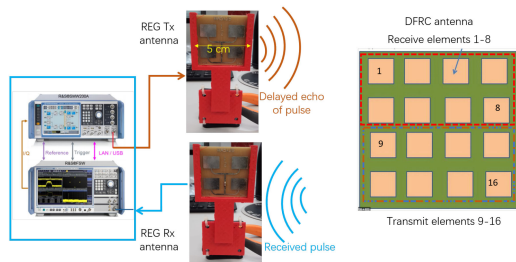Fig. 8. FPGA board, ADC cards and radio frequency card of the receiver.



Fig. 9. Schematic illustration of REG operation.

and up conversion, 8 waveforms are forwarded to the antenna array to be transmitted.

*3) DFRC Rx Board:* The receiver board allows the received radar echoes to be processed in software. Broadly speaking, it converts the passband analog echoes and received waveforms to baseband digital streams, forwarded to the server. The receiver board consists of a VC707 FPGA board, two FMC168 analog-to-digital convertors (ADCs) cards, and a radio frequency down-convertor board, as depicted in Fig. 8. Each received passband signal is first down converted to baseband by the radio frequency card. This process consists of amplifying the passband waveform, followed by being mixed with a local oscillator, and applying a baseband filter, resulting in a baseband signal, which is in turn amplified by a baseband amplifier. The amplified analog baseband waveform is converted to digital by the FMC168 card. The FMC168 is a digitizer featuring 8 ADC channels based on the TI ADS42LB69 dual channel 16-bit 250Msps A/D. The board is equipped with two ADC cards, where one is connected to the receive elements of the DFRC antenna and the other is connected to the communications receiver antenna. The high speed data transmission interface is implemented on the FPGA, transferring the signals to the PC server, where they are processed via the detection strategy detailed in Section II.

*4) REG:* In order to simulate echoes generated by moving radar targets in an over-the-air setup, we use a REG. The REG consists of a Rhode & Schwarz FSW signal and spectrum analyzer, which captures the received waveform, and a Rhode & Schwarz SWM200 A vector signal generator, which adds the delays and Doppler shifts to the observed waveform and transmits it over-the-air. The signal and spectrum analyzer and the vector signal generator are connected to a dedicated receive and transmit antenna element, respectively. The sizes of the REG receive and transmit antennas are 5 cm × 5 cm. An illustration of the REG components and their operation is depicted in Fig. 9. The REG operation is triggered when it receives a transmitted radar pulse. This procedure allows us to experiment our prototype with over-the-air signaling with controllable targets. Up to 6 targets can be generated by the REG, whose range and Doppler

can be configured to up to 10 kM and 190 kHz, respectively. The parameters of the targets are configured directly by the PC application by LAN interface.

*5) Data Processor:* The data processor is a 64-bit laptop with 4 CPU cores and a 16 GB RAM. A Matlab application operating on the data processor carries out the following tasks:

- Generation of the JRC waveform in digital, and forwarding them to the DFRC Tx board for transmission.
- Processing the received radar echoes, implementing the scheme detailed in Section II-D.
- Detection of the transmitted data symbol based on the received communications signal.

For experimental purposes, the application also provides the ability to embed a pre-defined target scheme into the received radar waveforms, allowing to evaluate the performance of the system with various configurable target profiles.

The processing flow and the configuration of the setup parameters are controllable using a dedicated GUI, as detailed in the following subsection.

### B. GUI: Configuration, Control, and Display

A GUI is utilized to configure the prototype parameters, control the experiment process, and display the results. A screenshot of the GUI is shown in Fig. 10.

*1) Parameter Configuration:* In order to simulate the DFRC system using the hardware prototype, one must first select the system configuration. The configurable properties of the system include radar parameters, communication parameters, and DFRC platform parameters. For the radar subsystem, the GUI allows to set the signal-to-noise ratio (SNR) of the radar echoes, i.e., the amount of noise added to the received waveforms in software, as well as the selection of the simulated target scenario mode. For the communications subsystem, one can specify the constellation order and the number of GSM symbols used. For the platform parameters, the GUI allows configuring the number of elements used in the antenna array, i.e., $M$, as well as how many antenna elements are assigned for radar or communications, i.e., $M_T^r$ and $M_T^c$.

*2) Controller:* Once the parameters are configured, an experiment can be launched. The GUI allows the user to launch an experiment in two stages, by first initializing the hardware components to use the specified parameters, after which the transmission and reception can begin. Once the experiment is on-going, its results are updated in real-time, and is carried out until either all waveforms have been transmitted, or, alternatively, it is terminated by the user.

*3) Displayer:* The experiment results are visually presented by the GUI using three figures which are updated in real-time, as well as an additional static figure displaying the locations of the simulated targets. For the evaluation of radar performance, the GUI compares SpaCoR with *Fix1* by dedicating a figure to each scheme. These figures can compare either the beam pattern, or the target recovery resolution. For communication evaluation, the BER curves of both methods are compared when transmitting at the same bit rate, i.e., the same number of bits per time slot.

## VI. NUMERICAL EVALUATIONS

In this section we evaluate SpaCoR and compare it to DFRC methods with fixed antenna allocation in hardware experiments
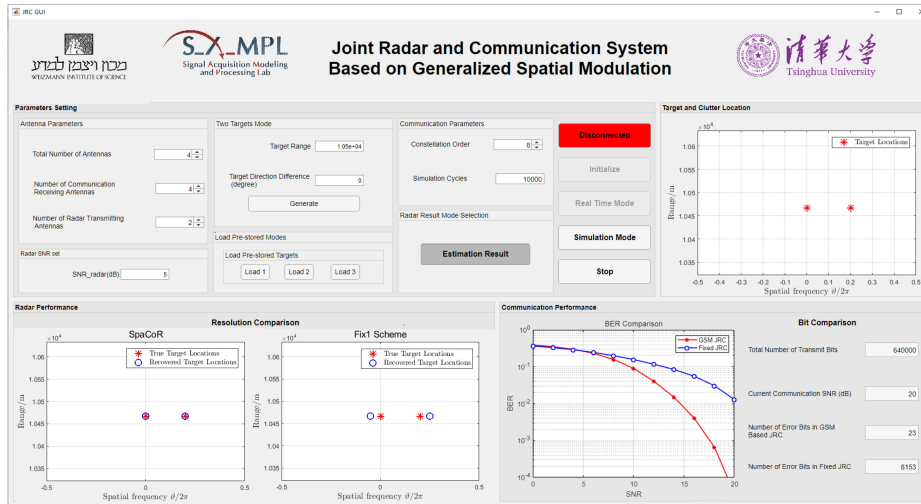
Fig. 10. Graphical User Interface of the prototype.

TABLE I
EXPERIMENT SETTINGS

| Parameter | Value |
|---|---|
| Number of total Tx elements $M$ | 4 |
| Radar pulse width $T_r$ | 30 $\mu s$ |
| Communication symbol duration $T_c$ | 2.5 $\mu s$ |
| Carrier frequency | 5.1 GHz |
| Radar frequency band | 5.06-5.11GHz |
| Communication frequency band | 5.11-5.14 GHz |
| DAC resolution | 16-bit |
| DAC update rate | 312.5 Msps |
| ADC resolution | 16-bit |
| ADC sampling rate | 250 Msps |

and simulations. The numerical evaluation of the radar and communications subsystems are detailed in Sections VI-A–VI-B, respectively. In particular, the radar performance in angular resolution detailed here is based on the hardware prototype, while the remaining evaluations are carried out in simulations. Table I lists some of the parameters used in our prototype-aided experiments. While the prototype allows using 8 antennas, in our experiments we use $M = 4$ elements. The REG receive antenna and transmit antenna are located at the normal direction of the DFRC transmit antenna with a distance of 0.5 m. The communications receive antenna is physically located within a similar distance from the DFRC system, but without direct line of sight to the DFRC transmit antenna. The prototype is evaluated in an indoor lab in the Weizmann Institute, with many devices and furniture, such that there are enough paths to form a rich-scattering environment which can be modeled as a Rayleigh channel.

## A. Radar Subsystem Evaluation

The analysis in Section III indicates that SpaCoR outperforms fixed antenna allocation schemes in several aspects: It has finer angular resolution compared with *Fix1* and has lower sidelobes compared with *Fix2*. In the following we demonstrate that these theoretical conclusions are also evident in our experiments,

We first compare the angular resolution of SpaCoR to *Fix1* by comparing their ability to recover the locations of multiple adjacent targets. Then, the angle of a radar target is estimated in the presence of interference caused by clutters, allowing us to evaluate the sidelobe levels of the different DFRC methods. Finally, we evaluate the performance of the radar subsystem for targets with various speeds, and SNR.

In the sequel, the bandwidth of radar waveform is set to $B_r = 50$ MHz. The locations of radar targets are recovered by using OMP [35] to solve (12). The number of radar Tx antenna elements is set to $M_T^r = 2$. The delay interval and the spatial frequency interval are set to $\delta\tau = \frac{1}{5B_r}$ and $\delta\vartheta = \frac{2\pi}{5M}$ in the evaluations of the radar angular resolution and the sidelobe level, while are set to $\delta\tau = \frac{1}{B_r}$ and $\delta\vartheta = \frac{\pi}{10M}$ in the simulation of the moving target scenario.

*1) Radar Angular Resolution:* The angular resolution determines the smallest angular distance required to distinguish two adjacent targets located in the same range cell. It is computed as half the width of the first two null points around the mainlobe of the beam pattern in the angular dimension. From the analysis in Section III-B, the angular resolution of SpaCoR is $\frac{2\pi}{M}$, which equals the angular resolution when using the full ULA with $M$ transmit antennas solely for radar. The resolution of *Fix1* is $\frac{2\pi}{M_T^r}$, which is larger than that of SpaCoR. To demonstrate that this advantage of SpaCoR over *Fix1* is translated to improved target recover, we consider a scenario with two targets located in the same range cell but with different angular directions. The direction of transmit beam is set to $\theta_T = 0$. In this experiment, we consider the noiseless scenario, and the reflective factors $\{\alpha_l\}$ are all set to one. Specifically, in the considered scenario the angular difference between the two adjacent targets is larger than the angular resolution of SpaCoR while smaller than the angular resolution of *Fix1*. The recovery results of SpaCoR and *Fix1* are shown in Fig. 11(a)–11(b), respectively, along with the true locations of the targets. From the recovery results, we observe that SpaCoR is capable of accurately recovering the target locations, while *Fix1* fails to do so. This is because that SpaCoR has improved resolution than that of *Fix1*. The recovery results of a more complex scenario with six targets are depicted in Fig. 12, which further demonstrates the
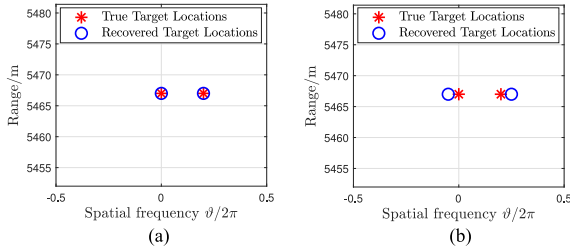
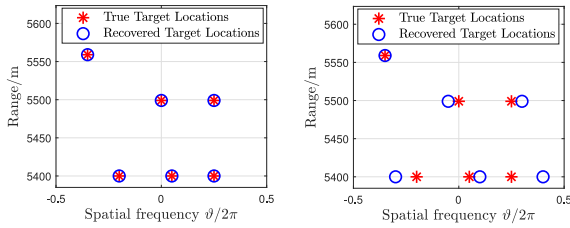Fig. 11. Recovery results for two adjacent targets.
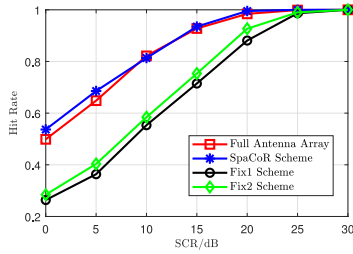


Fig. 12. Recovery results for six targets.



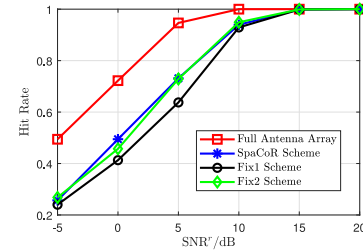Fig. 13. Hit Rate of angle estimate in different antenna allocation schemes versus different SCR.

TABLE II
TARGET PARAMETERS

| Target | Range | Speed |
|--------|--------|---------|
| 1 | 5545 m | 60 m/s |
| 2 | 5494 m | 240 m/s |
| 3 | 5401 m | 120 m/s |
| 4 | 5443 m | 180 m/s |
| 5 | 5365 m | 0 m/s |



Fig. 14. Hit rate of the range, angle and velocity estimates versus different $\mathrm{SNR}^r$.

improved ability of SpaCoR in identifying multiple adjacent targets.

*2) Sidelobe Level:* Radar target detection performance is degraded in the presence of clutters, where the magnitude of this degradation is related to the sidelobe level of the transmit beam pattern. A higher sidelobe level radiates more energy in the direction of the clutters, resulting in increased interference which in turn degrades detection performance. In Section III, we analyzed the sidelobe levels of SpaCoR and the fixed allocation schemes through the variance of transmit beam pattern. In this simulation, we demonstrate that the reduced sidelobe levels of SpaCoR translate into improved target detection accuracy. To that aim, we consider a scenario in which one radar target is located in the mainlobe of the radar transmit beam pattern, and evaluate radar performance in the presence of clutter. Two clutters are randomly generated outside the mainlobe of the transmit beam pattern in the same range cell with the radar target. The amplitudes of the clutter reflective factors are randomized following a Rayleigh distribution as in [44, Ch. 2.2].

Here, we use hit rate as the performance criterion. A "hit" is defined if the angle parameter of the target is successfully recovered. The hit rates of angle estimates are calculated over 4000 Monte Carlo trials versus the signal-to-clutter ratio (SCR), defined as the ratio between the square of target reflective factor and the square of the expected clutter reflective factor. The results are depicted in Fig. 13, where the hit rate curves of the full antenna array, SpaCoR, *Fix1* and *Fix2* are shown.

Observing these hit rate curves, we find that the hit rate of SpaCoR approaches that of using the full array, and outperforms the fixed allocation methods, while *Fix1* achieves the lowest hit rate for all considered SCR values. These results are in line with the theory analysis detailed in Section III: Due to the shrinkage of antenna aperture, the mainlobe of *Fix1* is wider than the mainlobes of SpaCoR and *Fix2*. Hence, the interference introduced by the clutters are strongest, which notably degrades the radar performance. SpaCoR outperforms *Fix2* as the variance of transmit beam pattern for SpaCoR is lower than that of *Fix2*, and thus its sidelobe levels are lower and it is less sensitive to interference caused by clutters.

*3) Moving Target Scenario:* In the previous experiments, we focused on the estimation of range and direction of the radar targets using one radar pulse. Nonetheless, when multiple pulses are transmitted, the radar subsystem can be easily extended to detecting moving targets as pulse Doppler radar [44, Ch. 5]. To evaluate the performance of the radar subsystem when detecting moving targets, we consider a scenario with five targets, which have different ranges, directions or velocities. All the targets are located in the mainlobe of the transmit beam. The range and velocity parameters of these targets are listed in Table II. One radar coherent processing interval (CPI) consists of $N_{\mathrm{CPI}}$ pulses, which is set to $N_{\mathrm{CPI}} = 5$. The reflective factors $\{\alpha_l\}$ of the targets are all set to one, and the amplitude of the transmit waveform is also set to be one.

Here, hit rate is used as the performance criterion. The parameters of the targets are recovered using the CS algorithm utilized in [45]. The radar signal-to-noise ratio is defined as $\mathrm{SNR}^r = \frac{\lfloor F_s T_r \rfloor}{\sigma_r^2}$. To evaluate the performance of radar subsystem under different noise levels, the hit rates of range, angle and velocity estimates are averaged over 4000 Monte Carlo trials versus $\mathrm{SNR}^r$. The angles of these targets are randomly generated from $\vartheta \in \left[-\frac{\pi}{M}, \frac{\pi}{M}\right]$, i.e., the angle range of the mainlobe, in each trial. The hit rate curves are shown in Fig. 14. We observe that the hit rate of the full antenna scheme, which utilizes the complete antenna array solely for radar, outperforms that of the other approaches. The DFRC schemes SpaCoR and *Fix2* achieve
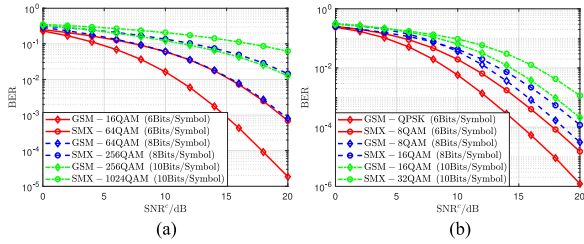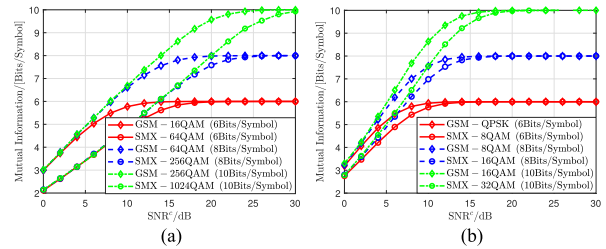
Fig. 15.  BER comparisons of GSM and SMX. (a) $M^c_T = 1$. (b) $M^c_T = 2$.



Fig. 16.  Mutual information comparisons of GSM and SMX. (a) $M^c_T = 1$. (b) $M^c_T = 2$.

almost the same hit rates which are better than the hit rate of *Fix1*. These results are in line with the analysis in Section III: In this experiment, the recovery performance is determined by the total transmit power and the width of the mainlobe. A higher transmit power and a thinner manilobe will lead to a better recovery performance. The full antenna array has the thinnest mainlobe and transmit the most power using all the antenna elements, thus has the best performance. While for SpaCoR and *Fix1*, the mainlobe width is equal to that of the full antenna array, while the fact that they transmit less power in radar signalling results in a small gap from the hit rate achieved when the full antenna array is utilized. Finally, since *Fix2* has the widest mainlobe, its hit rate performance is the worst among all considered schemes.

### B. Communications Subsystem Evaluation

The communication subsystem of SpaCoR is based on GSM signaling. For comparison, the DFRC systems with fixed antenna allocation do not encode bits in the selection of the antennas, and thus convey their information only via conventional spatial multiplexing MIMO (SMX). To compare the communication capabilities of the considered methods, we evaluate their uncoded BER performance, To that aim, a total of $10^6$ JRC waveforms are transmitted and decoded by the receiver. We evaluate the performances of both communication schemes by setting the number of communications transmit antennas as $M^c_T = 1$ and $M^c_T = 2$. To guarantee fair comparison, we set the data rates of the considered methods to be identical. For each setup with different number of transmit antennas, the data rates are set to be 6 Bits/Symbol, 8 Bits/Symbol and 10 Bits/Symbol, respectively. This is achieved by using constellations of different orders. In particular, when $M^c_T = 1$, we compare GSM-16QAM, which conveys two spatial bit in the selection of one antenna from an array of $M = 4$ elements, and four constellation bits, in the form of one 16QAM symbol, per GSM symbol, with SMX-64QAM. For other data rates and different number of transmit antennas, the constellations of orders are chosen in the similar way.

The BER curves of the GSM-based SpaCoR compared to DFRC systems with fixed antenna allocation utilizing SMX for communications are depicted in Fig. 15. We observe in Fig. 15(a) and Fig. 15(b) that for the same data rates, GSM achieves improved BER performance compared to SMX, and that its BER curve decreases faster than SMX with SNR. This gain follows from the fact that GSM utilizes less dense constellations compared to SMX, as it conveys additional bits in the selection of the antenna indices. Nonetheless, this performance gain comes at the cost of increased decoding complexity at the receiver, which is a common challenge associated with IM schemes.

The communication performance gains of GSM, observed in our evaluation of its uncoded BER performance, are also evident when evaluating its mutual information (MI) between the transmitted signal and the channel output, which represents its achievable rate. To demonstrate this gain, we numerically compare the MI of GSM with that of SMX in Fig. 16 using the same setups in the BER evaluations. Our evaluation of the MI values of GSM are based on the following equation [30]:

$$I\left(\mathbf{x}; \mathbf{y}\right) = -M^c_R \log_2 e$$
$$- \mathcal{E}_{\mathbf{H}} \left\{ \mathcal{E}_{\mathbf{y}|\mathbf{H}} \left\{ \log_2 \left( \frac{1}{2^\beta} \sum_{\mathbf{x} \in \mathcal{X}} e^{\frac{-\|\mathbf{y} - \mathbf{H}\mathbf{x}\|_2^2}{\sigma_c^2}} \right) \right\} \right\},$$

where $2^\beta$ is the cardinality of the set $\mathcal{X}$. The stochastic expectations are computed via empirical averaging. Similarly, the MI of SMX is obtained by substituting the corresponding input vector into (23). Observing Fig. 16(a), we note that, as expected, the MI does not exceed the number of bits encapsulated in each symbol. Consequently, when $M^c_T = 1$, the maximal MI of GSM-16QAM and SMX-64QAM equal 6 bits per symbol, the maximal MI of GSM-64QAM and SMX-256QAM equal 8 bits per symbol, while the maximal MI of GSM-256QAM and SMX-1024QAM equal 10 bits per symbol. However, these data rates can only be achieved reliably at high SNR values. In lower SNRs, GSM achieves improved MI over SMX, indicating that it is capable of reliably conveying larger volumes of data. When $M^c_T = 2$, similar results are observed in Fig. 16(b). These results, combined with the radar performance evaluated in Section VI-A, demonstrate that the usage of GSM in DFRC systems contributes to both radar, in its introduction of radar agility which contributes to the angular resolution, as well as the communications subsystem, allowing it to achieve improved performance in terms of both BER as well as achievable rate.

### VII. CONCLUSION

In this paper, we proposed SpaCoR, which is a DFRC system based on GSM. SpaCoR conveys additional bits by the combinations of transmit antenna elements, and the antenna allocation patterns change between symbols in a random fashion introducing spatial agility. The signal models and processing algorithms were presented. In order to evaluate the radar performance, we characterized the transmit beam pattern and analyzed its stochastic performance, showing that the beam pattern of the proposed system approaches that of using the full antenna array solely for radar. To demonstrate the feasibility of the approach, we built a dedicated hardware prototype realizing this DFRC system using over-the-air signaling. Hardware experiments and

simulations demonstrated the gains of the proposed method over DFRC systems using fixed antenna allocations in terms of both radar resolution and sidelobe level, as well as communication BER and achievable rate. Our results and the presented hardware prototype narrow the gap between the theoretical concepts of IM-based DFRC systems and their implementation in practice.

## APPENDIX

### A. Proof of Theorem 1

For a given time slot $k$, the indices of the radar transmitting antennas, denoted by $\mathbf{M}_k^{\text{GSM}}$, are randomized from the radar antenna combination set. The random vector $\mathbf{M}_k^{\text{GSM}}$ thus obeys a discrete uniform distribution over this set, i.e., $\Pr(\mathbf{M}_k^{\text{GSM}}) = 1/P_c$, where $P_c := \binom{M}{M_T^r}$ is the total number of possible antenna index combinations. The expected transmit delay-direction beam pattern can be calculated as follows:

$$
\mathcal{E}\left\{\chi_T^{\text{GSM}}(\tau_d, f_\theta)\right\} = \sum_{n=0}^{N_{\text{rec}}-1} \sum_{k=0}^{K-1} \mathcal{E}\left\{\rho_T(k, f_\theta)\right\}
$$
$$
\times g\left(\frac{nT_s - kT_c - \tau_d - \tilde{\tau}}{T_c}\right) h[n, \tau_d + \tilde{\tau}] h^*[n, \tilde{\tau}].
$$
$$
(\text{A.1})
$$

The expected value of the transmit gain in (A.1) is

$$
\mathcal{E}\left\{\rho_T(k, f_\theta)\right\} = \mathcal{E}\left\{\sum_{l=0}^{M_T^r-1} e^{jm_{k,l}f_\theta}\right\}
$$
$$
\overset{(a)}{=} \frac{1}{P_c}\sum_{i=0}^{P_c-1}\sum_{l=0}^{M_T^r-1} e^{jm_l^{(i)}f_\theta} \overset{(b)}{=} \frac{1}{P_c}\cdot\frac{P_c\cdot M_T^r}{M}\sum_{m=0}^{M-1} e^{jmf_\theta}
$$
$$
= e^{-j\frac{f_\theta}{2}}\cdot\frac{M_T^r}{M}\cdot\frac{\sin(Mf_\theta/2)}{\sin(f_\theta/2)}, \qquad (\text{A.2})
$$

where $(a)$ follows since $\mathbf{M}_k^{\text{GSM}}$ is uniformly distributed, and $(b)$ holds as there are $P_c \cdot M_T^r$ items in the summation, where each index in $\{0, 1, \ldots, M-1\}$ occurs $P_c M_T^r/M$ times. As $\mathcal{E}\{\rho_T(k, f_\theta)\}$ does not depend on the index $k$, we substitute $\mathcal{E}\{\rho_T(k, f_\theta)\}$ by $\mathcal{E}\{\rho_T(\cdot, f_\theta)\}$, and (A.1) is rewritten as

$$
\mathcal{E}\left\{\chi_T^{\text{GSM}}(\tau_d, f_\theta)\right\} = \mathcal{E}\left\{\rho_T(\cdot, f_\theta)\right\}
$$
$$
\times \sum_{n=0}^{N_{\text{rec}}-1} \sum_{k=0}^{K-1} g\left(\frac{nT_s - kT_c - \tau_d - \tilde{\tau}}{T_c}\right) h[n, \tau_d + \tilde{\tau}] h^*[n, \tilde{\tau}]
$$
$$
= \mathcal{E}\left\{\rho_T(\cdot, f_\theta)\right\}\cdot \sum_{n=0}^{N_{\text{rec}}-1} h[n, \tau_d + \tilde{\tau}] h^*[n, \tilde{\tau}], \qquad (\text{A.3})
$$

which follows from $\sum_{k=0}^{K-1} g(\frac{nT_s-kT_c-\tau_d-\tilde{\tau}}{T_c}) = g(\frac{nT_s-\tau_d-\tilde{\tau}}{T_r})$, and since $h(t)$ is a pulse with width $T_r$, $g(\frac{nT_s-\tau_d-\tilde{\tau}}{T_r})h[n, \tau_d + \tilde{\tau}] = h[n, \tau_d + \tilde{\tau}]$. Substituting (A.2) into (A.3) and taking its absolute values proves (17).

### B. Proof of Proposition 1

The variance of the transmit beam pattern is

$$
\mathcal{V} = \mathcal{E}\left\{\left|\chi_T^{\text{GSM}}(\tau_d, f_\theta)\right|^2\right\} - \left|\mathcal{E}\left\{\chi_T^{\text{GSM}}(\tau_d, f_\theta)\right\}\right|^2. \quad (\text{B.1})
$$

The second term in (B.1) is given in (17). By defining

$$
\eta(k, \tau_d) = \sum_{n=0}^{N_{\text{rec}}-1} g\left(\frac{nT_s - kT_c - \tau_d - \tilde{\tau}}{T_c}\right) h[n, \tau_d + \tilde{\tau}] h^*[n, \tilde{\tau}],
$$

it can be shown that $\mathcal{E}\{|\chi_T^{\text{GSM}}(\tau_d, f_\theta)|^2\}$ equals $\mathcal{E}\{\sum_{k=0}^{K-1}\sum_{k'=0}^{K-1}[\eta(k, \tau_d)\rho_T(k, f_\theta)\eta^*(k',\tau_d)\rho_T^*(k',f_\theta)]\}$, and can thus be written as

$$
\mathcal{E}\left\{\left|\chi_T^{\text{GSM}}(\tau_d, f_\theta)\right|^2\right\} = \sum_{k=0}^{K-1} |\eta(k, \tau_d)|^2 \mathcal{E}\left\{|\rho_T(k, f_\theta)|^2\right\}
$$
$$
+ \sum_{k=0}^{K-1}\sum_{k'\neq k} \eta(k, \tau_d)\eta^*(k', \tau_d)\mathcal{E}\left\{\rho_T(k, f_\theta)\rho_T^*(k', f_\theta)\right\}.
$$
$$
(\text{B.2})
$$

To compute (B.2), we note that by (4) and the fact that $\mathbf{M}_k^{\text{GSM}}$ obeys a uniform distribution, it holds that

$$
\mathcal{E}\left\{|\rho_T(k, f_\theta)|^2\right\} = \frac{1}{P_c}\sum_{i=0}^{P_c-1}\sum_{l=0}^{M_T^r-1}\sum_{l'=0}^{M_T^r-1} e^{j\left(m_l^{(i)}-m_{l'}^{(i)}\right)f_\theta}
$$
$$
\overset{(a)}{=} \frac{1}{P_c}\left\{\frac{P_c M_T^r(M_T^r-1)}{M(M-1)}\left|\sum_{m=0}^{M-1} e^{jmf_\theta}\right|^2 + \frac{P_c M_T^r(M-M_T^r)}{M-1}\right\}
$$
$$
= \frac{M_T^r(M_T^r-1)}{M(M-1)}\left|\frac{\sin(Mf_\theta/2)}{\sin(f_\theta/2)}\right|^2 + \frac{M_T^r(M-M_T^r)}{M-1},
$$
$$
(\text{B.3})
$$

where $(a)$ holds as the summation can be decomposed into constant terms, which add up to $\frac{P_c M_T^r(M-M_T^r)}{M-1}$, and to the term $|\sum_{m=0}^{M-1} e^{jmf_\theta}|^2$, which repeats $\frac{P_c M_T^r(M_T^r-1)}{M(M-1)}$ times. Additionally, for $k \neq k'$ the random variables $\rho_T(k, f_\theta)$ and $\rho_T^*(k', f_\theta)$ are independent, and thus

$$
\mathcal{E}\left\{\rho_T(k, f_\theta)\rho_T^*(k', f_\theta)\right\} = \left(\frac{M_T^r}{M}\right)^2\left|\frac{\sin(Mf_\theta/2)}{\sin(f_\theta/2)}\right|^2.
$$
$$
(\text{B.4})
$$

Furthermore, it holds that $\sum_{k=0}^{K-1}\sum_{k'\neq k}\eta(k, \tau_d)\eta^*(k', \tau_d) = |\sum_{n=0}^{N_{\text{rec}}-1} h[n, \tau_d + \tilde{\tau}]h^*[n, \tilde{\tau}]|^2 - \sum_{k=0}^{K-1}|\eta(k, \tau_d)|^2$. Substituting this as well into (B.1), we obtain

$$
\mathcal{V}\left\{\chi_T^{\text{GSM}}(\tau_d, f_\theta)\right\} = \sum_{k=1}^{K} |\eta(k, \tau_d)|^2 \times
$$
$$
\left\{\frac{M_T^r(M_T^r-M)}{M^2(M-1)}\left|\frac{\sin(Mf_\theta/2)}{\sin(f_\theta/2)}\right|^2 + \frac{M_T^r(M-M_T^r)}{M-1}\right\}.
$$
$$
(\text{B.5})
$$

When we specialize in (15) for chirp waveforms, it holds that $\sum_{k=0}^{K-1} |\eta(k,\tau_d)|^2 \approx \frac{N_r^2}{K}\text{sinc}^2(\frac{B_r\tau_d}{K})$. Utilizing this together with (18) proves (19). ∎

## REFERENCES

[1] D. Ma, T. Huang, Y. Liu, and X. Wang, "A novel joint radar and communication system based on randomized partition of antenna array," in *Proc. IEEE Int. Conf. Acoust., Speech, Signal Process.*, 2018, pp. 3335–3339.

[2] D. Ma, N. Shlezinger, T. Huang, Y. Liu, and Y. C. Eldar, "Joint radar-communication strategies for autonomous vehicles: Combining two key automotive technologies," *IEEE Signal Process. Mag.*, vol. 37, no. 4, pp. 85–97, 2020.

[3] B. Paul, A. R. Chiriyath, and D. W. Bliss, "Survey of RF communications and sensing convergence research," *IEEE Access*, vol. 5, pp. 252–270, 2017.

[4] G. C. Tavik *et al.*, "The advanced multifunction RF concept," *IEEE Trans. Microw. Theory Techn.*, vol. 53, no. 3, pp. 1009–1020, Mar. 2005.

[5] L. Han and K. Wu, "Joint wireless communication and radar sensing systems-state of the art and future prospects," *IET Microw., Antennas Propag.*, vol. 7, no. 11, pp. 876–885, 2013.

[6] L. Zheng, M. Lops, Y. C. Eldar, and X. Wang, "Radar and communication coexistence: An overview," *IEEE Signal Process. Mag.*, vol. 36, no. 5, pp. 85–99, Sep. 2019.

[7] Y. Liu, G. Liao, J. Xu, Z. Yang, and Y. Zhang, "Adaptive OFDM integrated radar and communications waveform design based on information theory," *IEEE Commun. Lett.*, vol. 21, no. 10, pp. 2174–2177, Oct. 2017.

[8] C. Sturm, T. Zwick, and W. Wiesbeck, "An OFDM system concept for joint radar and communications operations," in *Proc. IEEE Veh. Technol. Conf.*, 2009, pp. 1–5.

[9] F. Liu, L. Zhou, C. Masouros, A. Li, W. Luo, and A. Petropulu, "Toward dual-functional radar-communication systems: Optimal waveform design," *IEEE Trans. Signal Process.*, vol. 66, no. 16, pp. 4264–4279, 2018.

[10] F. Liu, C. Masouros, A. Li, H. Sun, and L. Hanzo, "MU-MIMO communications with MIMO radar: From co-existence to joint transmission," *IEEE Trans. Wireless Commun.*, vol. 17, no. 4, pp. 2755–2770, Apr. 2018.

[11] C. Sturm and W. Wiesbeck, "Waveform design and signal processing aspects for fusion of wireless communications and radar sensing," *Proc. IEEE*, vol. 99, no. 7, pp. 1236–1259, 2011.

[12] A. R. Chiriyath, B. Paul, and D. W. Bliss, "Radar-communications convergence: Coexistence, cooperation, and co-design," *IEEE Trans. Cogn. Commun. Netw.*, vol. 3, no. 1, pp. 1–12, Mar. 2017.

[13] Y. Zhang, Q. Li, L. Huang, and J. Song, "Waveform design for joint radar-communication system with multi-user based on MIMO radar," in *Proc. IEEE Radar Conf.*, 2017, pp. 0415–0418.

[14] E. Başar, "Index modulation techniques for 5G wireless networks," *IEEE Commun. Mag.*, vol. 54, no. 7, pp. 168–175, 2016.

[15] J. Wang, S. Jia, and J. Song, "Generalised spatial modulation system with multiple active transmit antennas and low complexity detection scheme," *IEEE Trans. Wireless Commun.*, vol. 11, no. 4, pp. 1605–1615, Apr. 2012.

[16] E. Başar, Ü. E. AygölüPanayırcı, and H. V. Poor, "Orthogonal frequency division multiplexing with index modulation," *IEEE Trans. Signal Process.*, vol. 61, no. 22, pp. 5536–5549, Nov. 2013.

[17] G. Kaddoum, Y. Nijsure, and H. Tran, "Generalized code index modulation technique for high-data-rate communication systems," *IEEE Trans. Veh. Technol.*, vol. 65, no. 9, pp. 7000–7009, Sep. 2016.

[18] F. Çogen, E. Aydın, N. Kabaoğlu, E. Başar, and H. Ilhan, "Code index modulation and spatial modulation: A new high rate and energy efficient scheme for MIMO systems," in *Proc. 41st Int. Conf. Telecommun. Signal Process.* 2018, pp. 1–4.

[19] E. Aydın, F. Çogen, and E. Başar, "Code-index modulation aided quadrature spatial modulation for high-rate MIMO systems," *IEEE Trans. Veh. Technol.*, vol. 68, no. 10, pp. 10 257–10 261, Oct. 2019.

[20] F. Çogen, E. Aydın, N. Kabaoğlu, E. Başar, and H. Ilhan, "Generalized code index modulation and spatial modulation for high rate and energy-efficient MIMO systems on rayleigh block-fading channel," *IEEE Syst. J.*, to be publsihed, doi: 10.1109/JSYST.2020.2993704.

[21] A. Hassanien, M. G. Amin, Y. D. Zhang, and F. Ahmad, "Dual-function radar-communications: Information embedding using sidelobe control and waveform diversity," *IEEE Trans. Signal Process.*, vol. 64, no. 8, pp. 2168–2181, Apr. 2016.

[22] A. Hassanien, B. Himed, and B. D. Rigling, "A dual-function MIMO radar-communications system using frequency-hopping waveforms," in *Proc. IEEE Radar Conf.*, 2017, pp. 1721–1725.

[23] X. Wang, A. Hassanien and M. G. Amin, "Dual-function MIMO radar communications system design via sparse array optimization," *IEEE Trans. Aerosp. Electron. Syst.*, vol. 55, no. 3, pp. 1213–1226, Jun. 2019, doi: 10.1109/TAES.2018.2866038.

[24] T. Huang, N. Shlezinger, X. Xu, Y. Liu, and Y. C. Eldar, "MAJoRCom: A. dual-function radar communication system using index modulation," *IEEE Trans. Signal Process.*, vol. 68, pp. 3423–3438, 2020.

[25] M. Bică and V. Koivunen, "Multicarrier radar-communications waveform design for RF convergence and coexistence," in *Proc. IEEE ICASSP*, 2019, pp. 7780–7784.

[26] P. M. McCormick, S. D. Blunt, and J. G. Metcalf, "Simultaneous radar and communications emissions from a common aperture, part I: Theory," in *Proc. IEEE Radar Conf.*, May 2017, pp. 1685–1690.

[27] X. Liu, T. Huang, N. Shlezinger, Y. Liu, J. Zhou, and Y. C. Eldar, "Joint transmit beamforming for multiuser MIMO communication and MIMO radar," *IEEE Trans. Signal Process,*vol. 55, no. 3, pp. 1213–1226, Jun. 2019.

[28] A. Younis, N. Serafimovski, R. Mesleh, and H. Haas, "Generalised spatial modulation," in *Proc. IEEE, Asilomar Conf. Signals, Syst. Comput.*, 2010, pp. 1498–1502.

[29] T. Huang, N. Shlezinger, X. Xu, D. Ma, Y. Liu and Y. C. Eldar, "Multi-Carrier Agile Phased Array Radar," *IEEE Trans. Signal Process.*, vol. 68, pp. 5706–5721, 2020, doi: 10.1109/TSP.2020.3026186.

[30] A. Younis and R. Mesleh, "Information-theoretic treatment of space modulation MIMO systems," *IEEE Trans. Veh. Technol.*, vol. 67, no. 8, pp. 6960–6969, Aug. 2018.

[31] F. Pérez-Cruz, M. R. Rodrigues, and S. Verdú, "MIMO gaussian channels with arbitrary inputs: Optimal precoding and power allocation," *IEEE Trans. Inf. Theory*, vol. 56, no. 3, pp. 1070–1084, Mar. 2010.

[32] M. I. Skolnik, *Introduction to Radar Systems*, 3rd ed. New York, NY, USA: McGraw-Hill, 2001.

[33] D. Cohen, D. Cohen, Y. C. Eldar, and A. M. Haimovich, "SUMMeR: Sub-nyquist MIMO radar," *IEEE Trans. Signal Process.*, vol. 66, no. 16, pp. 4315–4330, Aug. 2018.

[34] D. Cohen and Y. C. Eldar, "Sub-nyquist radar systems: Temporal, spectral, and spatial compression," *IEEE Signal Process. Mag.*, vol. 35, no. 6, pp. 35–58, Nov. 2018.

[35] Y. C. Eldar and G. Kutyniok, *Compressed Sensing: Theory and Applications*. Cambridge, U.K.: Cambridge Univ. Press, 2012.

[36] Y. C. Eldar, *Sampling Theory: Beyond Bandlimited Systems*. Cambridge, U.K.: Cambridge Univ. Press, 2015.

[37] B. Mailhe, R. Gribonval, F. Bimbot, and P. Vandergheynst, "A low complexity orthogonal matching pursuit for sparse signal approximation with shift-invariant dictionaries," in *Proc. IEEE Int. Conf. Acoust., Speech, Signal Process.*, 2009, pp. 3445–3448.

[38] C. Hu, Y. Liu, H. Meng, and X. Wang, "Randomized switched antenna array FMCW radar for automotive applications," *IEEE Trans. Veh. Technol.*, vol. 63, no. 8, pp. 3624–3641, Oct. 2014.

[39] I. G. Cumming and F. H. Wong, "Digital processing of synthetic aperture radar data," *Artech House*, vol. 1, no. 3, pp. 108–110, 2005.

[40] Y. Lo, "A mathematical theory of antenna arrays with randomly spaced elements," *IEEE Trans. Antennas Propag.*, vol. 12, no. 3, pp. 257–268, May 1964.

[41] A. Papoulis and S. U. Pillai, *Probability, Random Variables, and Stochastic Processes*. New York, NY, USA: Tata McGraw-Hill Education, 2002.

[42] M. Skolnik, *Radar Handbook, 3rd ed.*. New York, NY, USA: McGraw-Hill, 2008.

[43] M. Di Renzo, H. Haas, A. Ghrayeb, S. Sugiura, and L. Hanzo, "Spatial modulation for generalized MIMO: Challenges, opportunities, and implementation," *Proc. IEEE*, vol. 102, no. 1, pp. 56–103, Jan 2014.

[44] M. A. Richards, *Fundamentals of Radar Signal Processing*, 2nd ed. New York, NY, USA: McGraw-Hill, 2014.

[45] D. Ma, T. Huang, N. Shlezinger, Y. Liu, X. Wang, and Y. C. Eldar, "A DFRC system based on multi-carrier agile FMCW MIMO radar for vehicular applications," in *Proc. IEEE ICC Workshops*, 2020, pp. 1–7.

**Dingyou Ma** received the B.Sc. degree in aerospace science and technology from Xidian University, Xi'an, China, in 2016. He is currently working toward the Ph.D. degree with the Department of Electronic Engineering, Tsinghua University, Beijing, China. His current research interests include the system design and signal processing on dual-function radar-communications system.

**Nir Shlezinger** (Member, IEEE) received the B.Sc., M.Sc., and Ph.D. degrees in electrical and computer engineering from the Ben Gurion University of the Negev, Beersheba, Israel, in 2011, 2013, and 2017, respectively. From 2017 to 2019, he was a Postdoctoral Researcher with Technion–Israel Institute of Technology, Haifa, Israel, and from 2019 to 2020, he was a Postdoctoral Researcher with the Weizmann Institute of Science, Rehovot, Israel. He was the recipient of the FGS prize for Outstanding Research Achievements from the Weizmann Institute of Science. He is currently an Assistant Professor with the School of Electrical and Computer Engineering, Ben Gurion University of the Negev. His research interests include communications, information theory, signal processing, and machine learning.

**Tianyao Huang** received the B.S. degree in telecommunication engineering from the Harbin Institute of Technology, Harbin, China, in 2009 and the Ph.D. degree in electronics engineering from Tsinghua University, Beijing, China, in 2014. From 2014 to 2017, he was a Radar Researcher with the Aviation Industry Corporation of China, Beijing, China. Since July 2017, he has been an Assistant Professor with Intelligent Sensing Lab, Department of Electronic Engineering, Tsinghua University. His current research interests include signal processing, compressed sensing, and joint radar communications system design.

**Yariv Shavit** received the B.Sc.T.E. degree in electrical and communication engineering from Tel Aviv University (Holon branch), Tel Aviv, Israel, in 2001. From 1999, he was an Engineer in the industry, in particular 13 years as an Aerospace and Defense Application Engineer for Rohde & Schwarz. He was the SAMPL Lab Manager headed by Yonina Eldar, leading students projects, especially on radar, before joining back to the industry.

**Moshe Namer** received the B.Sc. degree in electrical and communication engineering from the Technion - Israel Institute of Technology, Haifa, Israel, in 1984. From 1984 to 2010, he was an Engineer with Communication Lab, Electrical Engineering Department, Technion, leading analog and RF circuits student projects in hardware implementations. Since 2010, he has been active with SAMPL Lab, headed by Yonina Eldar, working on hardware demo implementations.

**Yimin Liu** (Member, IEEE) received the B.S. (Hons.) and Ph.D. (Hons.) degrees in electronics engineering from Tsinghua University, Beijing, China, in 2004 and 2009, respectively. From 2004, he was with Intelligence Sensing Lab, Department of Electronic Engineering, Tsinghua University. He is currently an Associate Professor with Tsinghua University, where his field of activity is study on new concept radar and other microwave sensing technologies. His current research interests include radar theory, statistic signal processing, compressive sensing and their applications in radar, spectrum sensing, and intelligent transportation systems.

**Yonina C. Eldar** (Fellow, IEEE) received the B.Sc. degree in physics and electrical engineering from Tel Aviv University, Tel Aviv, Israel, in 1995 and 1996, respectively and the Ph.D. degree in electrical engineering and computer science from the Massachusetts Institute of Technology (MIT), Cambridge, MA, USA, in 2002.

She is currently a Professor with the Department of Mathematics and Computer Science, Weizmann Institute of Science, Rehovot, Israel. She was a Professor with the Department of Electrical Engineering, Technion–Israel Institute of Technology, Haifa, Israel, where she was the Edwards Chair in engineering. She is currently a Visiting Professor with MIT, a Visiting Scientist with the Broad Institute of MIT and Harvard, Cambridge, MA, USA, an Adjunct Professor with Duke University, Durham, NC, USA, and was a Visiting Professor with Stanford University, Stanford, CA, USA. She is the author of the book *Sampling Theory: Beyond Bandlimited Systems* and the coauthor of four other books published by Cambridge University Press, Cambridge, U.K. Her research interests include statistical signal processing, sampling theory and compressed sensing, learning and optimization methods, and their applications to biology, medical imaging, and optics.

She was the recipient of many awards for excellence in research and teaching, including the IEEE Signal Processing Society Technical Achievement Award (2013), the IEEE/AESS Fred Nathanson Memorial Radar Award (2014), and the IEEE Kiyo Tomiyasu Award (2016). She was a Horev Fellow of the Leaders in Science and Technology Program with the Technion–Israel Institute of Technology, Haifa, Israel and an Alon Fellow. She was the recipient of the Michael Bruno Memorial Award from the Rothschild Foundation, the Weizmann Prize for Exact Sciences, the Wolf Foundation Krill Prize for Excellence in Scientific Research, the Henry Taub Prize for Excellence in Research (twice), the Hershel Rich Innovation Award (three times), the Award for Women with Distinguished Contributions, the Andre and Bella Meyer Lectureship, the Career Development Chair with the Technion, the Murieland David Jacknow Award for Excellence in Teaching, and the Technions Award for Excellence in Teaching (two times). She was also the recipient of several Best Paper Awards and Best Demo Awards together with her research students and colleagues including the SIAM Outstanding Paper Prize, the UFFC Outstanding Paper Award, the Signal Processing Society Best Paper Award and the IET Circuits, Devices and Systems Premium Award, and was selected as one of the 50 most influential women in Israel and in Asia. She is also a highly cited Researcher. She was a Member of the Young Israel Academy of Science and Humanities and the Israel Committee for Higher Education. She is the Editor-in-Chief of *Foundations and Trends in Signal Processing*, a Member of the IEEE Sensor Array and Multichannel Technical Committee and was on several other IEEE committees. She was a Signal Processing Society Distinguished Lecturer, a Member of the IEEE Signal Processing Theory and Methods and Bio Imaging Signal Processing technical committees, and was an Associate Editor for the IEEE TRANSACTIONS ON SIGNAL PROCESSING, the *EURASIP Journal of Signal Processing*, the *SIAM Journal on Matrix Analysis and Applications*, and the *SIAM Journal on Imaging Sciences*. She was the Co-Chair and the Technical Co-Chair of several international conferences and workshops. She is a Member of the Israel Academy of Sciences and Humanities (elected 2017) and a EURASIP Fellow.